Investigations of Runaways in the Pulsator Tokamak

G.Fussmann und S.Sesnic

IPP III/37 August 1977

MAX-PLANCK-INSTITUT FÜR PLASMAPHYSIK

8046 GARCHING BEI MÜNCHEN

MAX-PLANCK-INSTITUT FÜR PLASMAPHYSIK

GARCHING BEI MÜNCHEN

Investigations of Runaways in the Pulsator Tokamak

G.Fussmann und S.Sesnic

IPP III/37 August 1977

Die nachstehende Arbeit wurde im Rahmen des Vertrages zwischen dem Max-Planck-Institut für Plasmaphysik und der Europäischen Atomgemeinschaft über die Zusammenarbeit auf dem Gebiete der Plasmaphysik durchgeführt.

IPP III/37

G.Fussmann
S.Sesnic

Investigations on Runaways in the Pulsator Tokamak

Abstract

This report reviews investigations of runaway electrons in the high-density discharges in Pulsator. Our analysis is based on the detection of hard X-rays (10 keV - 10 MeV) from the plasma and of those produced at the limiter by runaway bombardment. Detailed investigations were made during the initial phase of the discharge, at a time interval around the gas input, and during the disruption. During the initial phase we observe strong bursts of hard X-rays from the limiter and the liner wall with high integer q-values at the plasma boundary, caused by enhanced losses of runaways. It is found that most of the runaways produced during the current build-up phase are lost within the first 10 ms. The runaway production is then observed to increase with growing temperature until it is quenched by the gas input, which leads to a rapid increase of the electron density. Once the production of runaway ceases their confinement can be optimally studied. The experimental results indicate a global runaway confinement time of approximately 10 ms; the results are also in rough agreement with recent thoeries on the runaway production rate. In connection with the confinement of runaways a random walk loss model is discussed. The investigations of high-energy limiter radiation suggest preferential bombardment of the limiter outside, as predicted by the orbit shift model. On the other hand, this model does not describe the essential loss mechanism. We find many indications of enhanced loss processes, the most outstanding of which is the phase correlation of the hard X-ray intensity from the limiter with the saw-tooth oscillations connected with the internal disruptions. The main disruption itself is always preceded by a huge burst of hard X-rays in which all of the residual runaways with an energy of ~ 10 MeV are dumped on

the limiter. All observable radiation bursts are correlated with small jumps of the plasma current, presumably indicating a rearrangement of the current density distribution.

Contents

I. Introduction

Investigations of runaways were taken up soon after Pulsator was put into operation, and meanwhile an extensive amount of data has been gathered. A short preliminary report has already been published /1/. Concerning the presence of runaways, the history of Pulsator discharges can be summarized as follows: During the initial period of operation large amounts of runaways were produced in the discharges. These high production rates were caused by the relatively low conductivity of the plasma, which in turn was a consequence of the impurities in the vessel. After a few thousand shots, after which the machine had become considerably cleaner, it was observed that the runaway production had been reduced, too. With further improvement of the degree of purity, however, difficulties with runaways were again incurred. This time high production rates were reached after a few times 10 ms in the discharge, this being due to a decrease of the electron density. The decrease of density during a shot is a natural consequence of the finite particle confinement time and a recycling coefficient less than 1. Under unclean conditions, however, this effect is usually overcompensated by a flux of light impurities from the walls. Finally, in the case of Pulsator, the situation became rather severe: After about 70 ms many discharges turned into the runaway dominated phase, which is characterized by an uncontrolled decrease of the loop voltage. During the same time a series of runaway instabilities with a repetition rate of approximately 1 - 2 ms was observed. These instabilities are distinguished by positive voltage spikes and strong bursts of hard X-rays with a duration of several tens of μs. In order to overcome this undesirable situation we were forced to look for some means by which the electron density could be increased. We finally succeeded in using a fast input of hydrogen gas. By means of this procedure we got rid of the actual runaway problems and, in addition, obtained discharge conditions which are best suited to studying the confinement of the remaining runaways[+].

[+] A summary of the high-density operation of Pulsator is given in Ref. /2/.

In the following only this type of discharge will be discussed. In particular, we shall concentrate on three important intervals:

- the initial phase of the discharge
- a time interval before and after the gas input
- the disruption phase.

II. Hard X-ray diagnostic system

The hard X-ray system used for the analysis of runaway plasma radiation is shown in Fig.1. The spectral analysis of the radiation is performed by means of a 3" x 3" NaI crystal to which a photomultiplier is attached. This unit is accommodated in a lead housing with a wall thickness of 8 cm and an exchangeable input aperture (3-20 mm in diameter). A second aperture is situated about 1 m away and can also be exchanged in order to adjust the hard X-ray flux. Additional lead shielding reduces the scattered radiation from the copper shell, the iron transformer etc., and in particular the radiation coming directly from the limiter. The whole system is positioned in the toroidal direction on the opposite side of the limiter. Photons from the plasma (with energies < 3 MeV) have to go through a diagnostic shaft and a Be window to reach the detection system. For a photon energy exceeding 10 keV the transparency of the window is greater than 84 %. The detection system can be tilted so that one can scan over the inner minor radius of the plasma.

It is very important to know whether the observed radiation is from the plasma or from the surrounding walls. In our case, the system always "sees" a small part of the liner surface, which is radially only 3 cm in the shade of the limiter. To clarify the origin of the radiation, experiments with a movable tungsten sphere(8 mm in diameter) were performed (see Sec. III.1)

The voltage pulses from the photomultiplier are fed into a pulse height analysis system. The digitized signals are sent

to a PDP-11 computer, where the pulses are stored in an array of 256 x 4000 bytes. The 256 channels yield information about the photon energy and the 4000 channels give the time information. In this way we obtain time resolved energy spectra. For statistical optimization we can integrate over some time and energy intervals and sum up an arbitrary number of shots.

III. Investigations of runaway phenomena

III.1 Runaways during the initial phase

First we discuss the start-up phase of the discharge. In Fig.2a we present oscilloscope traces of the plasma current, the loop voltage, and hard X-ray pulses for the first 9 ms of the discharge. Figure 2b likewise shows the loop voltage and, in addition, the derivative of the plasma current for the same type of discharge with a higher time resolution. The current plateau of 48 kA is reached after about 3 ms. During this time the loop voltage decreases from 60 to about 3 V. The traces of the plasma current and the loop voltage (measured with a toroidal loop at the major radius $R_L = R_o - 18$ cm) allow us to calculate the electric field outside the plasma. In cases where the plasma current or the current density profile changes, the loop voltage inside and outside the plasma may be quite different owing to inductive effects. Estimates of these inductive effects show that during the initial phase the electric field at the plasma centre can be appreciably smaller than at the boundary, but since the actual current density profiles are unknown and hence the time integral of the electric field as well, the factor of uncertainty remains too large to permit decisive retracing to the time of origin of a runaway whose energy has been measured.

Some information on the electron density and temperature at the early times of the discharge are given in Fig.3 /3/. This shows

that the plasma is already fully ionized at about 0.5 ms. At the same time the first hard X-rays with a maximum energy of approximately 100 keV appear (Fig. 2a). As time goes on, the maximum energy of the photons increases to ~ 1 MeV and there are bursts in the intensity which are correlated with rapid changes in the loop voltage. As can be seen from Fig.2b, these changes in the loop voltage are exactly correlated with inverse changes of the current derivative, where the latter signal has been slightly integrated with a time constant of 36 µs; the original signal of the current derivative is strongly disturbed by fluctuations with a characteristic frequency of 200 kHz. Even more important, the spikes in the loop voltage correspond to decreasing integer values of the safety factor q_a within the limits of experimental error (~ 5 %), when a slightly reduced plasma radius of 10.5 cm is assumed instead of the limiter radius a = 11 cm. It is very remarkable that q_a-values as high as 15 can be identified.

It should be noted, however, that such a definite identification of integer q_a-values is only possible under the conditions stated. Increasing the rise time of the plasma current from 3 ms to 7 ms or decreasing it to 1 ms leads to smaller voltage spikes where the high q_a-numbers ($q_a \gtrsim 7$) do not show up and the identification of the $q_a < 7$ numbers becomes less certain.

From Fig. 2a one can deduce that the $q_a = 5$ value is run through twice (at 3.3 and 5.9 ms). Both events coincide with the appearance of hard X-rays with energies of about 1 MeV[+)]. In order to determine the origin of the radiation bursts the aperture in front of the Be window was closed with a lead plug for a number of shots. No photons could be detected in these cases for the first 10 ms. Thus, it has been verified that these radiation bursts come from either the plasma or the liner surface but not from the limiter. The only reasonable explanation for the intensity bursts, however, is a runaway bombardment of the wall, otherwise we should have to postulate that the target density

+) Some of the radiation bursts were also observed with a second detection system looking perpendicularly to the limiter. As the limiter, however, is hidden behind a few cm of shielding walls only the bursts with high photon energies can be detected with this system.

(i.e. $Z_{eff} \cdot n_e$) is enormously increased within time intervals as small as 100 μs. Moreover, this interpretation is supported by investigations with the tungsten sphere shown in Fig.1. If this sphere was brought 2 cm into the limiter shadow, the W-K_α radiation at 60 keV could be observed during the first 3 ms when looking at the sphere from above (Fig.4a and 5b). At later times, however, this characteristic radiation could not be detected (Fig.5a and 5b). There are some differences in the experiments with and without the tungsten sphere. Figure 6 shows a polaroid with the hard X-ray pulses from the W sphere as well as the inverted loop voltage and the current flowing from the sphere. The latter signal is not very reproducible, and we shall not comment further on it. In contrast to the measurements described previously, there is just one very strong burst of radiation appearing prior to the spikes in the loop voltage. The quiet period without radiation activity following the burst can last as long as 20 ms. It should be mentioned, however, that there have also been series of shots where the initial bursts decrease continuously in intensity although the machine was operated under the same conditions; thus it appears that these early bursts appear preferentially under relatively less clean conditions.

We have not yet found a conclusive and fully convincing interpretation that would explain all of our observations. A possible interpretation is the following:

- Most of the runaways are generated in a small time interval around 0.3 - 0.4 ms. This is the time when a small rotational transform ($q_a \lesssim 100$) is already efficient in confining the particles but the loop voltage is still very high. Neglecting inductive effects, the electric field is about 0.1 V/cm at this time and the runaways get 80 keV in 100 μs. According to our interferometer measurements (Fig.3) the plasma is already fully ionized at this time. The temperature is estimated to be about 10 eV only, but a high non-Maxwellian tail must be assumed.

- The runaway production takes place in an outer shell of the plasma because the highest electric fields are to be expected there owing to the skin effect. This runaway shell leaks out towards the wall as a consequence of magnetic islands being created in connection with MHD modes. The MHD modes observed in the experiment with high integer q_a-values have the character of surface modes and are likely to be excited on account of strong gradients of the current density at the plasma.

- We assume that most of the runaways are lost at the limiter but at least a certain fraction has also been found to reach the liner wall. In this connection the elastic scattering from the limiter (even for 1 MeV electrons the back-scattering coefficient for a thick Mo target is as large as 20 %; see Ref. /4/) may play a crucial role. Particles scattered from the limiter have the chance to exchange their large parallel momentum into perpendicular momentum and are thus susceptible to trapping processes into some local magnetic mirrors[+].

III.2 Current plateau phase

III.2.1 Quenching of the runaway production

The time development of the four plasma parameters that determine the runaway production is given in Fig. 7. The central values for the electron temperature and the electron density as well as Z_{eff} were obtained from Thomson scattering. U_L is the loop voltage. The hydrogen gas is added at 40 ms and the corresponding particle flux has a characteristic rise time of 5 ms. This gas input reaches the plasma centre about 10 ms later. In most cases this type of discharge is disrupted by an instability which sets in between 80 and 120 ms.

If the n_e and T_e profiles are known, the runaway production rate profiles $S(r,t)$, can be calculated. Such profiles, calculated on the basis of the theory given by Connor and Hastie /6/ which has

[+] Trapping of hot electrons, induced probably by some instability mechanisms has been observed in particular in the TFR Tokamak /5/.

been absolutely adjusted to the calculations of Kulsrud /7/ (for numerical details see Fef. /8/), and assuming Z_{eff} to be independent of r, are shown in Fig. 8 for several times. Because of the sensitivity of the production rate to small changes in temperature and density, only profiles of T_e and n_e measured in the same series of shots can be used to correlate with hard X-ray measurements. In Fig. 8 we show profiles of the production rate where the solid lines were obtained by taking an average of the two values at $R_o + r$ and $R_o - r$. The dashed lines in Fig. 8 are calculated using data for $R_o + r$ only; therefore, and because of the reduced accuracy of the n_e and T_e measurements close to the boundary this part of the profiles is rather unreliable. In general, however, we see from Fig. 8 that the runaway production profiles are relatively broad up to about 30 ms but become more peaked afterwards, since with increasing temperature the temperature profile peaks, too.

The total production rate of runaways S_{tot} within the torus can be obtained from the S(r) profiles . It is shown in Fig. 9 for several times. The total production rate becomes negligible soon after the density increases in the centre. The calculation yields a decrease of the runaway production rate by about twelve orders of mangitude towards the end of the discharge. For the purpose of comparison with theory, the production rate is approximated by an exponential increase and an abrupt quenching at t = 50 ms (Fig. 9). In order to calculate from the production rate the number of runaways in the torus at any particular time, an assumption about their confinement must be made. Ad hoc we introduce a runaway confinement time τ_r and assume the probability that a runaway born at time t_o is still in the discharge at time t to be $P(t,t_o) = e \times p\left[-(t - t_o)/\tau_r\right]$. No justification for this assumption can be given but in the next section we shall show that it is compatible with a random walk loss model. The total number of runaways with τ_r as a parameter, i.e. $N_{tot}(t) = \int_o^t S_{tot}(t_o) \cdot P(t,t_o)dt_o$, is also shown in Fig. 9.

Furthermore, we give in the same figure the calculated minimum energy of the runaways (6 MeV), the runaway current, and the energy contents of the runaways for t = 85 ms.

III.2.2 Random walk loss model

Let us consider the following model: A runaway created at a certain radius at a certain time undertakes a random walk over the cross-section in the course of which its parallel momentum is increased. If the particle once touches the limiter it is lost.

This statistical process can be described by a diffusion equation with a formal diffusion coefficient D. According to this, the equation for the runaway distribution function f(q,p,t) is given by

$$\frac{\partial f}{\partial t} - \frac{1}{a^2 \rho} \frac{\partial}{\partial \rho} D \rho \frac{\partial f}{\partial \rho} + \frac{1}{\tau} \frac{\partial f}{\partial \tilde{q}} = 0 \quad , \quad \tilde{q} > 0 \tag{1}$$

Here $\tilde{q} = (p-p_c)/m_o c$ is the normalized momentum of the particles, p_c is the critical momentum for runaway generation, $\rho = r/a$ the normalized radius, and $\tau = m_o c/eE$ is a characteristic time defined by the electric field $E = U_L/2\pi R_o$ (m_o = electron rest mass, e = elementary charge, c = velocity of light). In addition to eq. (1) we have the boundary conditions $f(\rho = 1) = 0$ and $f(\tilde{q} = 0) = \tau S(\rho,t)$; the latter condition is obtained by means of $dt = \tau\, d\tilde{q}$. The total number of runaways at a given time is obtained from

$$N_{tot}(t) = 2\pi a^2 R_o \int_0^1 d\rho\, 2\pi\rho \int_0^\infty d\tilde{q}\, f(\tilde{q},\rho,t) \tag{2}$$

Assuming as a first approach that the diffusion coefficient is independent of energy, time and radius, the general solution of the problem is given by a Fourier-Bessel series:

$$f(\tilde{q},\rho,t) = \sum_{\nu=1}^{\infty} A_\nu(\tilde{q},t) \exp\left(-\frac{D\xi_\nu^2}{a^2}\tau\tilde{q}\right) J_o(\xi_\nu \rho) \tag{3a}$$

with

$$A_\nu(\tilde{q},t) = \frac{2\tau}{J_1^2(\xi_\nu)} \int_0^1 S(\rho, t-\tilde{q}\tau)\, J_o(\xi_\nu\rho)\, \rho\, d\rho \tag{3b}$$

where $\xi_\nu = 2.40, 5.52...$ are the zeros of J_o. From eq.(3b) we see that for a given momentum $\tilde{q}$ the coefficients A_ν are defined by the runaway production at the retarded time $t_o = t - \tilde{q}\tau$. With growing momentum the terms with $\nu > 1$ decay very rapidly in eq. (3a) and the only remaining term is that of lowest order. Thus, the radial profiles tend to become the Bessel profile $J_o(\xi_1 \rho)$. If the runaway production is substantial only within a small time interval at t_o (as is approximately the case in our experiment), we have $A_\nu \propto \delta(\tilde{q} - \frac{t-t_o}{\tau})$ and from eq. (3a) it can be deduced that the high energy tail ($\tilde{q} > 1$) decays exponentially with a time constant

$$\tau_r = \frac{a^2}{D\xi_1^2} \qquad (3c)$$

which may be termed as the runaway confinement time.

As has already been mentioned, the diffusion constant D is just a quantity that describes the random walk of the particles perpendicular to the magnetic field lines and has little or nothing to do with the classical diffusion constant. The random walk could be caused by, for example, radial $\vec{E} \times \vec{B}$-dirfts on account of fluctuating poloidal electric fields, as has been discussed by **Spitzer**/9/ to account for anomalous diffusion in stellarators. From this point of view it would not be surprising if τ_r turns out to be comparable with the confinement time of thermal electrons (~ 5 ms at high densities in Pulsator) since the $\vec{E} \times \vec{B}$ drift velocity is independent of the particle energy. For the diffusion coefficient one obtains /9/

$$D = \frac{\langle \Delta r^2 \rangle}{\Delta t} = 2\,\frac{\langle E_{pol}^2 \rangle}{B^2 \tau_s}\,, \qquad (4)$$

where τ_s is the self-correlation time, i.e. the characteristic time during which the electric field in the frame of the moving particle does not change essentially ($\tau_s \gg 1/\omega_{gyro} = 2 \cdot 10^{-12}$ s must be assumed). To get an idea of the magnitude of the field we assume $\tau_r = 10$ ms in eq. (3c) and quite

arbitrarily $\tau_s = 1\,\mu s$ in eq. (4); we get $D = 2 \cdot 10^3 cm^2 s^{-1}$ and $\sqrt{\langle E^2_{pol} \rangle} \sim 0.1$ V/cm. Since the wavelength in the poloidal direction is limited to $\lambda \leq 2\pi a$, this field strength could be supplied by a potential difference of $\Delta\phi \leq \lambda \sqrt{\langle E^2_{pol} \rangle} = 6.9$ V, which is rather small compared with thermal energies $kT_e/e \sim 10^3$V.

Another mechanism yielding radial transport of the particles is caused by the formation of magnetic islands and by ergodization of the magnetic field lines. In the case of ergodization, any point within a finite volume can be reached by following a magnetic field line. Some experimental evidence for ergodization has been found in the Australian LT-3 tokamak /10/. Localized ergodization takes place at the boundary of magnetic islands, which are created by helical perturbation currents inside or outside the plasma. Within a magnetic island the radial transport is caused by the fact that a magnetic field line changes from the inside of the island to the outside after a number of turns around the torus (depending on the magnetic shear, typical values are ~ 10). Helical perturbations have been observed in Pulsator as in most tokamaks on the q = 1 and q = 2 surfaces, but smaller island formations must be visualized also for intermediate rational q-values, especially for q = 3/2, 5/2. Large scale ergodization can be established by overlapping of magnetic islands /11,12/

III.2.3 Analysis of plasma radiation

Our experimental data comprises X-ray emissivities integrated over a chord of the plasma

$$I(k,t,b) = \int \varepsilon \, dl = 2 \int_0^1 \frac{\varepsilon(k,t,\rho)}{\sqrt{\rho^2 - b^2}} \rho \, d\rho \qquad (5)$$

as a function of the photon energy k, the time t, and the distance of the chord from the plasma centre b. These intensities are defined by the number of photons per second, per solid angle element $\Delta\Omega$, per surface element ΔS and

divided by the relative photon energy interval $\Delta k/k$, i.e. $I = \dot{N}_{Ph} \cdot k/\Delta k \cdot \Delta S \cdot \Delta \Omega$. Within the energy interval 50 keV $\leq k \leq$ 500 keV the measured spectra can be well described by an exponential law

$$I(k,t,b) = I_o(t,b) \cdot \exp\left[-\frac{k-k_o}{k_c}\right] , \qquad (6)$$

where I_o is the integrated intensity at k_o = 50 keV and k_c is the characteristic energy defining the slope of the spectrum. Hence, the extensive data can be represented by showing graphs of I_o and k_c versus time for various chord distances, as shown in Figs. 10 and 12. In Fig. 10 we see that after the initial burst (described in Sec. III.1) I_o increases again, as is to be expected from the increase of the runaway production. At the time of the gas input the intensity decreases almost instantaneously at the plasma edge and about 10 ms later at the plasma centre. After this time the intensity curves for the different chords run approximately parallel, which means that the radial profile does not change any more. This is in general agreement with the above theoretical model, but the measured profile is much more peaked than the theoretical one, where the intensity is assumed to be proportional to $n_e(\rho) \cdot J_o(\rho \cdot \xi_1)$. Figure 11 gives an example of the discrepancy between theory and experiment for t = 57.5 ms. This disagreement could be due to an increase of the diffusion coefficient towards the plasma boundary (possibly caused by magnetic islands).

In Fig.12 we see that up to 50 ms k_c slowly increases and is practically constant over the plasma cross-section. Thereafter k_c increases quickly with the highest values towards the boundary. Here we have to point out, however, that for the outer chords large errors are present with the tendency to increase k_c. These are due to the low intensities obtained for the off-centre chords and to the growing background of the limiter radiation becoming gradually hard enough to penetrate the lead shielding.

In order to get some information on the runaway confinement time, it is convenient to define a normalized intensity over the central chord by

$$H(k,t) = \frac{I(k,t,b=0)}{Z_{eff}(t) \cdot n_{e_0}(t)} \quad . \tag{7}$$

Here again no concentration of impurity is assumed, and the effective charge density of the nuclei $\tilde{Z}_{eff} = \Sigma_n Z^2_n n_n / \Sigma_n Z_n n_n$ has been replaced by the effective ion charge density $Z_{eff} = \Sigma_i Z^2_i n_i / \Sigma_i Z_i n_i$, which is correct only in the case of complete ionization. However, since the predominant impurity in Pulsator is fully ionized oxygen, the two quantities do not differ very much in practice; the ratio $\tilde{Z}_{eff}/Z_{eff}$ was estimated to be 1 - 1.5.

The experimental function H_{exp} is obtained from the central intensity and laser scattering data. This is to be compared with the asymptotic (taking only the term $\nu = 1$ of eq. (3) into account) theoretical function

$$H_{theor}(k,t) = 2\rho_1 a c \tau \int_{T_{min}>k}^{T_{max}} Q(k,t) \cdot S_o[t - \tau\tilde{q}(T)] \cdot \exp\left[-\frac{\tau\tilde{q}(T)}{\tau_r}\right] dT \,, \tag{8}$$

where $Q = \frac{k\, d^2\sigma}{dk\, d\Omega}$ is the bremsstrahlung cross-section for a photon emission angle of 90° (we use eq. (2BN) of Ref. /13/ with the Elwert correction), S_o the central runaway production rate, T the kinetic energy of the runaways, and ρ_1 the effective normalized radius which can be determined from the measured profile I(b) according to

$$\rho_1 \equiv \int_0^1 \frac{\varepsilon(\rho)}{\varepsilon(0)}\, d\rho = -\pi \left[2\int_0^1 \frac{I'(b)}{I(0)}\, \frac{db}{b}\right]^{-1} \geq \int_0^1 \frac{I(\rho)}{I(0)}\, d\rho \,, \tag{9}$$

with I' = dI/db. The right-hand side approximation of eq.(9) holds for strongly peaked profiles.

The bremsstrahlung cross-section as a function of kinetic energy for various photon energies and $\theta = 90°$ is shown in Fig. 13. The

decrease of the cross-section with growing kinetic energy is due to the fact that the radiation becomes more and more peaked in the forward direction. In addition, we give in Fig. 14 the cross-section for a photon energy of 50 keV and the characteristic slope energy k_c versus kinetic energy. Here the bremsstrahlung cross-section has been approximated by an exponential law $Q \propto \exp(-k/k_c)$, which can be done for the range 50 keV $\leq k \leq$ 500 keV. The curves of Fig. 14 are very useful if a quick check of a measured spectrum is to be made.

Equation (8) is only correct for a Bessel profile of the production rate. In the case of homogeneous production the right-hand side of eq.(8) is to be multiplied by 1.6. Thus, correction factors are not substantial and will be neglected. In Fig. 15 experimental results for a photon energy of 50 keV (where experimental errors are smallest) are compared with numerically calculated values of H_{theor}. Because of the rather large inaccuracies in the absolute values of H_{theor} one should first refer to the slopes of the functions. Comparing these for $t > 60$ ms, a runaway confinement time decreasing from 50 to less than 10 ms could be deduced. For several reasons, however, it would be an overintepretation to draw such detailed conclusions from Fig. 15. One important fact is the discontinuity of the runaway loss induced by the gas input and also the discontinuities caused by the internal disruptions, as will be discussed in the next sections. Another point is that the measured spectrum at t = 57.5 ms shows a much steeper slope than the caluclated spectra for $\tau_r \geq 10$ ms, whereas for t = 67.5 ms both spectra agree fairly well if $\tau_r = 10$ ms is assumed. Hence, it seems to be more realistic to deduce from Fig. 15 a global runaway confinement time of approximately 10 ms. The same value for the runaway confinement time has been found in the ST tokamak (R_o = 109 cm, a = 13 cm) by considering the steady-state runaway distribution /14/. In addition, for this confinement time we also get fairly good agreement for

the absolute values. Although the observed agreement is better than is to be expected (the factor of uncertainty is about 5 - 10), we do not see any reason to distrust the calculations of runaway production rates as deduced from measurements in the ST tokamak. In connection with this question, it should be noted that from a rigorous point of view it is almost impossible to distinguish in the experiment between low production rate and high loss rates as the actual loss mechanisms are unknown. Thus, if there is,for example, enhanced loss of runaways in the range of ~ 100 keV at the limiter, this loss is generally not detectable because of too thick absorbers and the background radiation from higher energy runaways; consequently, too low a production rate would be deduced from the experiment.

Finally, we want to emphasize that in Pulsator the shots with the lowest hard X-ray intensities (no photons above 1 MeV are observed) are not believed to have very low production rates but suffer from poor confinement; they are always characterized by a high but strongly fluctuating loop voltage.

III.2.4 Hard X-rays from the limiter

Recently some supplementary measurements of the limiter radiation were performed. Some of these measurements were made with the set-up shown in Fig.16. The radiation from the limiter inside and outside was simultaneously detected with two identical systems. Because of a transformer yoke, the very tangential direction for the limiter inside is not accessible in Pulsator, and the measurements were made under the smallest possible angle of 17^{o} with regard to the runaway velocity vector at the limiter. By means of test absorbers (Fig.16) it could be verified that this double system is very effective in discriminating between the limiter outside and inside, as far as scattering at the torus structure can be neglected. For the interpretation of the measurements it is very important that all absorbers around the machine are care-

fully taken into account. Adding up the contributions from the copper shell, coils, vacuum vessel etc. we have 1 cm Fe, 3.8 cm Cu and 5.8 cm Fe, 11.3 cm Cu for the limiter inside and outside, respectively. Thus, the radiation from the limiter outside is about 70 to 25 times more attenuated than the radiation from the inside with reference to photons of 2-10 MeV (see Table I).

A record of a typical shot is shown in Fig. 17. The first hard X-rays ($k > 1$ MeV) appear at about $t = 35 - 40$ ms. Right after the beginning of the gas puff the intensities are appreciably increased for about 5 - 10 ms, and small fluctuations in the loop voltage, similar to those observed during the initial phase, occur. This phase of enhanced limiter radiation is always succeeded by a period of low intensity. After this, the intensity increases again to reach a maximum at about 90 ms.

Taking into account the different attenuation factors for the two beams, we get roughly 100 times as much radiation from the outside as from the inside for $t \gtrsim 40$ ms. It is also observed that the radiation from the outside is somewhat more energetic. The increase of the intensity at the time of the gas input indicates obviously enhanced loss processes. In contrast, however, to the observations at the disruption phase no correlation between the intensity bursts from the limiter inside and outside are found at these times. From this we conclude that the intensity of the inner beam is not due to Compton scattering only (which is otherwise known to be of great importance), but is caused by runaway bombardment of the limiter inside. In addition, it should be noted that at the time of the gas puff the plasma is generally strongly pushed inward by about 1 cm by a programmed step in the vertical magnetic field[+)]. In spite of this, the highest intensities are obtained from the limiter outside.

[+)] This step has proved to be of advantage in avoiding disruptions at these early times.

There is a general agreement between our observations and those made by the Ormak group /15/, which also found that high-energy runaways are preferentially lost at the limiter outside. The explanation for this given by the Ormak group is based on the orbit shift model, according to which the runaway drift surfaces are shifted outwards owing to the curvature drift velocity $v_d = v_{\parallel}^2 / R_o \omega_g$ (with gyro-frequency $\omega_g = eB/\gamma m_o c$ relativistic parameter $\gamma = (1 - v^2/c^2)^{-1/2} = 1 + T/m_o c^2$ and $v_{\parallel}$ the velocity paralel to $\vec{B}$). Neglecting toroidal effects, this shift is given by

$$\Delta x = r \frac{v_d}{v_{pol}} = \frac{m_o c^2}{e B_{tor}} \bar{q} \gamma \beta_{\parallel} \sim 0.056 \bar{q} \sqrt{\gamma^2 - 1} \quad [cm] \qquad (10)$$

with $\bar{q} = \bar{r} B_{tor} / R_o B_{pol}$ and $\beta_{\parallel} = v_{\parallel}/c \sim \beta = v/c$ Equation (10) holds in particular for a flat current profile (q = const) where the drift orbits are concentric circles in the minor cross-section. For peaked current profiles the shift can be appreciably reduced, but the orbits became somewhat elongated, too. For realistic current profiles, however, the shift of the orbit centre is always much more important than its deformation. From a more detailed analysis of the drift equations, we find that in the case of Pulsator the deviations from circular orbits are less than 5 % up to energies of 10 MeV for a current density profile $j \propto [1-(r/a)^2]^3$. In those cases the orbit radius is practically conserved and it is identical with the radius r_o of the poloidal flux surface on which the runaway was produced. The shift is then obtained from eq. (10) by setting $\bar{r} = \sqrt{r_o^2 + \Delta x^2}$.
For T=5 MeV electrons we get a shift as large as 1.8 cm for particles produced on the q = 3 surface ($r_o \sim 10$ cm, a = 11 cm, $I_p = 60$ kA $B_{tor} = 30$ kG). Thus the orbit shift model can indeed explain the preference of the limiter outside with respect to runaway bombardment. On the other hand, this model does not apply for the real loss mechanism since it fails to explain how the runaways that were found concentrated at the plasma centre in Sec. III.2 can get from the centre to the outer regions.

Another observation made at Ormak and considered as confirmation of the shift model /15/ is the onset of the limiter bombardment

with the decrease of the plasma current. Similar effects have also been observed in Pulsator but more precise measurements showed that generally the onset takes place when the current is still slightly increasing; if there is such a current criterion at all, it seems to be $\ddot{I}_p > 0$ rather than $\dot{I}_p < 0$ according to our measurements. An example of such a measurement - recorded with a single NaI detector looking to the limiter outside at 17° - is shown in Fig. 18 (in Fig. 17 $\ddot{I}_p > 0$ coincides with the intensity increase at t = 68 ms). We also have difficulties in explaining this effect quantitatively by means of eq. (10). There is, of course, the tendency for $\bar{q}$ to increase if the plasma current decreases, but there is also always a shift increment due to the energy increase of the runaways. Quantitatively, we get

$$\frac{d\Delta x}{dt} = \Delta x \left(\frac{1}{\tau \sqrt{\gamma^2 - 1}} - \frac{\dot{I}_p}{I_p} \right) \quad , \tag{11}$$

where $\tau = m_o c/eE$ is again the characteristic acceleration time (see Sec. III.2.2) during which relativistic runaways gain 0.5 MeV. In Pulsator we have for the quasi current plateau under consideration $\tau \sim 3$ ms and $\dot{I}_p/I_p \sim -1/300$ ms. Thus, the first term in eq.(11) is always much larger than the second one since extreme relativistic particles $\gamma > 21 \;\hat{=}\; 10$ MeV can be excluded.

Let us consider in more detail the stopping mechanism of the runaways at the limiter. Relativistic runways need only some 10ns (15 ns in Pulsator) for a torus revolution. Within this time no significant changes on the MHD time scale can take place. It is therefore most likely that runaways hit the very edge of the limiter outside (in Pulsator a 0.6 cm thick circular Mo diaphragm with rounded edge) when they first touch it. However, as it is known that the range of MeV electrons is of the order of a millimeter in molybdenum (e.g. 1.6 mm for 4 MeV; see Ref./4/), the runaways are probably not absorbed at their first impact. On the other hand, it can be assumed that the perpendicular velocity of the particles is considerably increased even in relatively weak limiter interactions, resulting in an increase of the gyroradius, too. From the relation

$$r_g = \frac{v_\perp}{\omega_g} = \frac{m_o c^2 \gamma \beta_\perp}{e B_{tor}} = 0.06\, \gamma \beta_\perp \; [cm] \quad , \tag{12}$$

we see that the gyro-radius can become several millimetres for relativistic particles ($2 \lesssim \gamma \lesssim 20$) as $\beta_\perp = v_\perp/c$ approaches unity. Now, the particle can penetrate much deeper into the limiter the next time it comes close to its outside edge. We have to note, however, that in the case $\beta_\perp / \beta_\parallel > \sqrt{R_o/2a} = 1.8$ the particles will be trapped and much larger shifts are to be expected (in eq. (10) $\beta_\parallel$ is to be replaced by $\beta_\perp \sqrt{R_o(1-\cos\theta_t)/a}$, with $\pm\,\theta_t$ being the angles of the turning points). As trapping is assumed to be an exceptional case, we will not consider it in the following. Thus, referring to a circular geometry, the distance of the guiding centre of the particles to the limiter boundary after n toroidal revolutions is given approximately by

$$\delta_n = \Delta x\,(1-\cos\theta_n)\,, \qquad \frac{\Delta x}{a} \ll 1\,, \tag{13}$$

where $\theta_n = n 2\pi/\bar{q}_a$ is the poloidal angle in the limiter plane, and $n = 0$, $\theta_o = o$ corresponds to the first impact at the outside, assuming $r_g(n=0)$ to be negligible. The condition for the second impact is $\delta_n \leq r_g$, or by means of eqs.(10)-(13)

$$1-\cos\theta_n \leq \frac{\beta_\perp}{\beta_\parallel \bar{q}_a}\,. \tag{14}$$

Thus, the maximum angle under which a non-trapped runaway can hit the limiter the second time is given by

$$\cos\theta_{max} = 1 - \frac{\sqrt{2R_o/a}}{\bar{q}_a}\,. \tag{15}$$

As an example let us consider the case $\bar{q}_a = 3.6 = 18/5$. For this we get $\theta_{max} = \pm\,32^o$ and because of $\theta_n = n \cdot 100^o$ the runaways perform at least seven revolutions ($\theta_7 = -20^o$) between the first and the second impact. Another part, however, will need 11 revolutions ($\theta_{11} = +20^o$) for the second impact and those with smaller $\beta_\perp$ need as much as 18 ($\theta_{18} = 0^o$). If we take into account an uncertainty in $\bar{q}_a$, a broadening of the impact angles is obtained. For $q_a = 3.6 \pm 0.02$,

for example, we get $\theta_7 = -20^\circ \pm 4^\circ$, $\theta_{11} = +22^\circ \pm 2^\circ$, $\theta_{18} = 0 \pm 10^\circ$ and $\theta_{n>18} = 0 \pm 6^\circ$. Some runaways will perform more than two impacts before they finally get stuck in the limiter. All these particles will deposit their energy at some preferential domains at the limiter outside with $|\theta| < |\theta_{max}|$.

No such details of the limiter bombardment are known from the experiments. However, well localized melting spots at the limiter outside, coinciding with the positions of activation due to (γ, n) processes, have been found in the TFR and PLT tokamaks /16,17/. The activation clearly indicates that there has been bombardment by high-energy runaways at these places. In contrast to this, we find the limiter in Pulsator to be damaged almost all over its periphery and slightly activated (E.Glock, priv. communication) at both the outside and the inside, although the plasma is generally well centered. As the limiter has been in use for several thousands shots, we do not know whether melting is a common or a more accidental phenomenon. On the other hand, the activation must have occurred during the last ~100 shots (high density) before opening the torus since the radioactivity decayed rather rapidly and could be detected only for a few days. Runaways impinging on the limiter inside possibly indicate an ergodization of the magnetic field lines in the outer plasma regions.

Because of the undefined conditions in the runaway-limiter interaction, the limiter radiation is not very well suited to quantitative analysis. In addition to the general problems with thick target bremsstrahlung, there is no well defined target thickness in this case. Therefore, only the high energy part of the bremsstrahlung spectra, for which reabsorption in the target becomes negligible, can be used for analysis. Furthermore, there is a lack of information concerning thick target bremsstrahlung. Most of the available data /18-23/ refers to the radiation in the forward direction and applies to W, Al, or Fe targets. For targets above or equal to the optimal thick-

ness, there is only a weak dependence of the bremsstrahlung intensity on the Z of the target material (see Ref./21/) for the high-energy part of the spectrum, but the peaking of the radiation in the forward direction is still appreciable, though much less pronounced in comparison with the thin target case. The quantity usually given in the literature is the bremsstrahlung yield $\frac{d^2y}{dk d\Omega}(T,k,\Theta)$ (photons/MeV · ster · electron) for optimal target thickness. By means of this quantity we get an approximate relation for the number of runaways impinging per time interval on the limiter, $\dot{N}_r$, and the pulse rate $\dot{N}_p$ obtained from the detector

$$\dot{N}_p(t) = \mathcal{H} \cdot \Delta\Omega \cdot A[T(t)] \cdot \dot{N}_r \qquad (16a)$$

with

$$A(T) = \int_0^T \eta(k) \cdot \tau(k) \cdot \frac{d^2y}{dk\,d\Omega}\, dk \,. \qquad (16b)$$

In this equation $\tau(k)$ is the transparency function of the various absorbing materials, $\eta(k)$ the total detector efficiency, and $\mathcal{H} \leq 1$ is a geometry factor accounting for the fact that usually not the total limiter periphery is observed. By means of equation (16) it is possible in principle to determine the runaway confinement time from the measured pulse rate since the kinetic energy is rather well known as a function of time in the high-density case:

$$\tau_r = \frac{-(t_2 - t_1)}{\ln(A_1 \dot{N}_{p1} / A_2 \dot{N}_{p2})} \,. \qquad (17)$$

Unfortunately, no data for the bremsstrahlung yield at $\Theta = 17^\circ$ and 2 MeV $\lesssim T \lesssim$ 12 MeV has been found in the literature.

Another point that has to be taken into account is the poor detector responsivity to photons above 1 MeV. Although the total detection efficiency η for the 3" x 3" NaI crystals is larger than 60 % for all energies, the photopeak efficiency

becomes less than 10 % for photons above 5.5 MeV /24,25/. Hence, the photon energy-pulse height relation given in the figures is to be understood in the sense that the detected photon has at least the energy given by the pulse height.

III.2.5 Correlation of high-energy radiation with internal disruption

A very informative discovery, namely the correlation of the hard X-ray radiation with the saw-tooth oscillation of the internal disruption, was made very recently in Pulsator. This correlation was first observed when utilizing fast plastic scintillators behind a limiter pin-hole camera /26,27/. So far the correlation could only be detected at high densities ($n_e \gtrsim 7 \cdot 10^{13} cm^{-3}$) when the saw-tooth amplitude is large and the period becomes about 1 ms or greater. There was first some uncertainty whether the observed oscillation is to be attributed to limiter or plasma radiation. By means of a NaI crystal in a telescope mounting it could be verified, however, that the oscillation appears in the limiter radiation at energies above $\sim$ 1 MeV. This is in agreement with estimates according to which the plasma-radiation intensity is at maximum 1 % of the limiter radiation intensity in the runaway forward direction at the limiter for k $\geq$ 1 MeV (photons of lower energy are strongly absorbed in the torus structure) if a runaway confinement time of 10 ms is assumed. In Fig. 19 we show a trace of the hard X-ray intensity in comparison with the soft X-ray signal obtained from a surface barrier diode looking through the centre of the plasma. The hard X-ray signal is the pulse rate from a NaI system collimated to the limiter outside with an observation area 4 cm in diameter. As can be seen from Fig.19, there is an inverse saw-tooth oscillation in the hard X-ray limiter radiation: Soon after the soft X-ray intensity has dropped, the hard X-ray intensity has its maximum. Unfortunately, the details are smoothed out because of the relatively long integration time of 1 ms needed in the case of the hard X-rays.

These observations throw a new light on the so-called internal disruption, which is generally considered to be a phenomenon confined to the inner part of the plasma where $q \lesssim 1$. From our measurements,however, we conclude that there is also a long range effect extending to the plasma boundary ($q_a \sim 5$ in these experiments) or even beyond. This is deduced from the fact that right after the internal disruption, when the temperature in the plasma centre has suddenly dropped, relativistic runaways strike at the limiter. One can speculate that these runaways come from the centre of the plasma and are able to do so because of a magnetic ergodization induced by the internal disruption.

III.3 Observations of runaways in high-density external disruptions

Because of its great importance, particularly for the high-density case, the disruption phase has been extensively studied in Pulsator. These investigations were reported at the IAEA-Conference in Berchtesgaden (1976) /28/. In order to classify our recent observations, it seems suitable to give a brief summary of those previous measurements and interpretations: In Fig. 20 we show various signals for a time interval of 0.5 ms around the disruption. The lower half of the picture shows soft X-ray signals (surface barrier diodes) for different chords. In the upper half we see from above to below: the plasma current, two traces of the loop voltage (the first with low and the second with high sensitivity), hard X-ray pulses from the limiter (observed at 90°) , and two signals from Mirnov coils showing the activity of the $m = 2$ mode. The disruption itself is characterized by a large negative voltage spike and is accompanied by a drop of the temperature, deduced from the central soft X-ray signals. In most cases only a single burst is observed, but there are others where up to five bursts, synchronized with the $m = z$ oscillation, appear. Usually, after the first disruption consecutive disruptions occur, separated from each other by about 200 μs. However, no hard X-ray bursts are observed in these subsequent disruptions.

From these observations and some additional information from pick-up coils the following interpretation was derived: A few ms before the disruption, the m = 2 mode couples with the m = 1 mode and the coupled system performs a uniform toroidal rotation with a frequency of typically 15 kHz. The amplitudes of both modes slowly increase and so, consequently, do the magnetic islands associated with them. The disruption is initiated by the touching of the two islands. At this time particles from the inside of the plasma can reach the outside just by following the magnetic field lines. The drift surfaces of the runaways are displaced outward. Therefore the runaways are preferentially lost - at the outer part of the limiter - when the rotating islands intersect the midplane of the torus. As the perturbation grows deeper and deeper layers of runaways are depleted at each rotation of the system (leading to several bursts). This depletion is already completed at the time of the negative voltage spike. Moreover, a major loss of thermal particles immediately before the negative voltage spike sets in.

Our previous experimental findings have been generally confirmed by more recent measurements made with the double system shown in Fig. 16. Indeed, a hard X-ray burst is always observed preceding the negative voltage spike, which indicates the disruption. Frequently this first observable voltage spike is much smaller than the consecutive ones, as can be seen from Fig. 21b. In some cases these subsequent voltage spikes are also correlated with weak X-ray bursts, but generally only one burst is observed. The main burst is always simultaneously seen from both the outside and inside parts of the limiter with approximately equal intensities which, however, does not necessarily mean that the runaway fluxes are equal (see below). An example of such a measurement is shown in Fig.21a, where the burst appears about 200 μs (typical values are 50 μs) prior to the negative voltage spike (showing cut-off due to finite range of transient recorder). Pulses due to single photons within the burst can be distinguished, though some pulses slightly overlap. The highest photon energies for disruptions occurring at t = 110 ms have been found to be $\sim$ 10 MeV for both the outside and the inside channels. This fits

quite well to the assumption of a free fall acceleration of runaways ($T = \left(\sqrt{1+(\Delta t/\tau)^2}-1\right) m_o c^2$, with $\tau = 3$ ms) being produced at $t_o = 50$ ms, i.e. immediately before the runaway production rate is assumed to be quenched. For the interpretation of the intensities observed in the two channels the different attenuations must again be taken into account (see Sec. III.2.4). In Table I we give the transmission values $\tau(k) = \exp\left[-\sum \mu_i(k) \rho_i x_i\right]$ for the limiter outside and inside channel (with 3 cm lead in front of the detector apertures) and, in addition, the calculated photon yield of T = 10 MeV electrons for $\Theta = 0^o$ and $\Theta = 12^o$ of a thick tungsten absorber /23/. Because of the much stronger attenuation in the limiter outside line, we conclude that also at the disruption most runaways hit the limiter outside. The question whether there is runaway bombardment of the limiter inside at all, or whether the observed intensity is purely due to scattering in the torus structure cannot be definitely answered.

It is important to have an idea how many runaways hit the limiter during a disruption burst. This number can be roughly estimated by means of eq. (16), using the second last and last lines of Table I as well as $\eta \sim 0.65$ for the integration over the photon energy in eq. (16b). Integrating eq. (16a) over the time interval of the burst, we get a relation between the number of runaways ΔN_r and the number of pulses occurring in the outside detector ΔN_p. With $\Delta N_p \sim 10$, $\Delta\Omega = 1.6 \cdot 10^{-6}$ ster and $\varkappa \sim 0.5$ we obtain $\Delta N_r = 5 \cdot 10^{10}$. As there are no runaways to be observed later on, ΔN_r is identical with the total number of runaways N_{tot} in the torus at the time of disruption (t = 110 ms). Comparing this value with the calculated number at t = 50 ms (see Fig. 9) a runaway confinement time of 6 ms is obtained. With regard to the various inaccuracies, this value is in rather good agreement with the 10 ms found in Sec. III.2.3. The current carried by the runaways at the time of the disruption $I_r = e \cdot c \cdot N_r / 2\pi R_o$ = = 0.5 A is completely negligible. This confirms our previous assumption that the runaway burst does not induce the disruption, but is merely its first indication.

In addition to the X-ray pulses and the loop voltage, we show the derivative of the plasma current in Fig. 21a. This signal is available with a high time resolution ($\sim 7\,\mu s$) as measured with a Rogowski coil inside the liner. As can be seen from the polaroid, there is a current increase of approximately 150 A associated with the X-ray burst. Obviously, this increase cannot be attributed to the runaway loss at the limiter since in this case a decrease rather than an increase of the current is to be postulated. Indeed, a current decrease of a fraction of I_r (we estimate $\Delta I_r/I_r \sim 0.3$) should show up in a time much smaller than the skin time (~ 5 ms) because of the differences in the inductances of the runaway current (being a surface current at the time of limiter quenching) and the plasma current. Hence, the observed current increase must be of totally different origin. A possible reason might be a sudden broadening of the current density profile leading to a decrease of the plasma inductance. Assuming poloidal flux conservation at the plasma centre $\Phi_{pol}(r=0) = I_p \cdot L_p(r=0)$, the plasma current has to go up, and outside of the plasma a decrease of the loop voltage is to be measured.

IV. Conclusions

It is found that during the current build-up phase many runaways are produced. They can only gain relatively low energy because they are poorly confined. Enhanced losses of runaways, associated with bombardment of the wall, are observed at high integer values of the safety factor. Trapping of runaways in the local magnetic mirrors is a possible but still questionable explanation of the wall bombardment since in the case of Pulsator the magnetic field ripple is only 0.3 %. Whatever the reason for the wall bombardment may be, one has to realize that this process may introduce impurities into the plasma.

The initial phase ends with a minimum in the hard X-ray intensity at about 15 ms. Thereafter the intensity increases owing to the increase of the runaway production rate up to the time of the gas input. After the gas input the runaway production is quenched and the hard X-ray intensity decreases exponentially. The intensity profiles are strongly peaked in the centre and the characteristic energy of the spectra increases towards the boundary. Comparison of normalized intensities with calculated intensities yields the loss rate of runaways. Assuming a confinement probability according to $\exp\left[-(t - t_o) / \tau_r\right]$ (where t_o is the time of birth), the loss can be expressed in terms of the runaway confinement time τ_r. $\tau_r \sim 10$ ms is deduced from the comparison between theory and experiment.

The runaway loss is also observable at the limiter when the radiation becomes sufficiently energetic. We find enhanced losses at the time of the gas input and later on a correlation of the hard X-ray limiter radiation with the saw-tooth oscillation of the internal disruptions. Most of the runaways are lost at the limiter outside, as predicted by the orbit shift model. This model does not, however, describe the mechanism by which the particles are driven from the plasma centre to the boundary layers.

The main disruption shows many similarities to the internal disruptions and appears in some way as a very strong internal disruption. On the other hand,there is no temporal correlation between the main disruption and the preceding internal disruption: Frequently, the main disruption occurs immediately after an internal disruption. In contrast to the internal disruption we always observe a burst of hard X-rays preceding the drop of temprature.

Furthermore, it is observed that the radiation burst at the disruption coincides with an increase of the plasma current, which can be explained by means of flux conserving arguments, in terms

of current profile broadening. Applying the same arguments to the initial phase, the positive voltage spikes and the negative jumps of the current can be attributed to shrinkage of the current profile. In both cases MHD or resistive instabilities, causing radial heat and particle transport by island formation (Ref. /11,12), are considered to be the driving mechanisms.

A possible - but not the only conceivable - interpretation of the observed imperfect confinement of the runaways is a radial ergodization of the magnetic field lines: Generally, this ergodization is very weak and the particles can perform several million toroidal turns before impinging on the limiter or the wall of the vessel. Under the influence of MHD and resistive modes, however, the ergodization in some domains of the torus may be considerably increased so that part of the runaways are already lost after a few thousand or even fewer revolutions.

Acknowledgement:

The authors wish to express their gratitude to the Pulsator Team: only in a close collaboration with the whole team was it possible to make these investigations. We would like to thank Dr.G.von Gierke for his suggestions and comments in the course of the studies. Special thanks are extended to Dr.E.Glock of the Pulsator Team with whose pin hole camera set up the sawteeth in the hard X-rays from the limiter were first observed.

References

/1/ S.Sesnic and G.Fussmann, IPP III/29 (1976):
Runaway Bremsstrahlung Spectra in the Pulsator Tokamak

/2/ O.Klüber, IPP III/21 (1976):
High Density Operation in Pulsator

/3/ W.Engelhardt, priv. communication

/4/ P.J.Ebert et al., Phys.Rev. 183, 2, 422-430 (1969)

/5/ Equipe TFR, EUR-CEA-FX-801 (1975):
electrons découplés et diffusion anormale des electrons piegés dans les miroirs locaux du Tokamak TFR

/6/ J.W.Connor and R.J.Hastie, Nucl.Fus. 15, 415 (1975)

/7/ R.M.Kulsrud et al., Phys.Rev.Lett.31, 690 (1973)

/8/ G.Fussmann, IPP III/30 (1976):
Generation and Dynamics of Runaway Electrons in Tokamaks

/9/ L.Spitzer, JR., Phys.Fluids, 3, 659-661 (1960)

/10/ J.D.Strachan, Nucl.Fusion 16, 743-751 (1976)

/11/ J.M.Finn, MATT-1137 (1975):
The Destruction of Magnetic Surfaces in Tokamaks by Current Perturbations

/12/ A.B.Rechester and T.H.Stix, MATT-1168:
Magnetic Braiding Due to Weak Asymmetry

/13/ H.W.Koch and J.W.Motz, Rev.Mod.Phys. 31, 4 (1959)

/14/ S.v.Goeler et al., Third Intern.Symp.on Toroidal Plasma Confinement (Garching 1973) paper B-25

/15/ H.Knoepfel and S.J.Zweben, Phys.Rev.Lett., 35, 20 B40 (1975)

/16/ T.F.R.Group, Phys.Lett.A, 60, 3, 219 (1977)

/17/ J.D.Strachan et al., Princeton University, TM-296 (1976):
Photo Neutron Production in the PLT Tokamak

/18/ A.A.O'Dell, JR. et al., Nucl.Inst.a.Math., 61, 340-346 (1968)

/19/ A.Powell, JR., NASA TN D-4755 (1968):
Tables of Energy and Angular Distributions of Thick Target Bremsstrahlung in Metals

/20/ W.Wayne Scott, NASA TN D-4063 (1967:
Angular Distributions of Thick-Target Bremsstrahlung which Includes Multiple Electron Scatterings

/21/ W.C.Dickinson and E.M.Lent, UCRL-50442 (1968):
Calculation of Forward Bremsstrahlung Spectra from Thick Targets

/22/ H.Ferdinande, Nucl.Instr.and Math., 91, 135-140 (1971)

/23/ M.J.Berger and S.M.Seltzer, Phys.Rev. C, 2, 2, 621-631 (1970)

/24/ H.E.Knoepfel et al., ORNL-TM-5022 (1975):
Hard X-ray Detection System for Ormak

/25/ B.Grosswendt and E.Waibel, Nucl.Instr. and Math., 133, 25-28 (1976)

/26/ E.Glock et al., Bull. Am. Phys. 22, 1201 (1977)

/27/ E.Glock, to be published

/28/ F.Karger et al., IAEA-CN-35/A7
Plasma Physics and Controlled Nuclear Fusion Research (1976)

/29/ K.Siegbahn, "Alpha-, Beta- and Gamma-Spectroscopy", Vol.I, Appendix I, North-Holland (1965)

TABLE I

K [MeV]	0.5	1	1.5	2	3	4	5	6	7	8	9	10
$\mu_{Pb}\rho_{Pb}$ [cm^{-1}]	1.803	0.798	0.591	0.518	0.475	0.472	0.480	0.491	0.504	0.519	0.534	0.552
$\mu_{Cu}\rho_{Cu}$ [cm^{-1}]	0.744	0.524	0.426	0.374	0.319	0.295	0.282	0.276	0.273	0.271	0.272	0.273
$\mu_{Fe}\rho_{Fe}$ [cm^{-1}]	0.660	0.470	0.382	0.334	0.283	0.260	0.246	0.239	0.235	0.233	0.232	0.231
τ_{inside}	$1.4\cdot10^{-4}$	$7.9\cdot10^{-3}$	$2.3\cdot10^{-2}$	$3.7\cdot10^{-2}$	$5.4\cdot10^{-2}$	$6.1\cdot10^{-2}$	$6.3\cdot10^{-2}$	$6.3\cdot10^{-2}$	$6.2\cdot10^{-2}$	$6.0\cdot10^{-2}$	$5.7\cdot10^{-2}$	$5.4\cdot10^{-2}$
$\tau_{outside}$	$2.2\cdot10^{-8}$	$1.6\cdot10^{-5}$	$1.6\cdot10^{-4}$	$4.8\cdot10^{-4}$	$1.3\cdot10^{-3}$	$2.0\cdot10^{-3}$	$2.5\cdot10^{-3}$	$2.7\cdot10^{-3}$	$2.7\cdot10^{-3}$	$2.7\cdot10^{-3}$	$2.5\cdot10^{-3}$	$2.4\cdot10^{-3}$
$\frac{d^2y}{dk\,d\Omega}(\Theta=0°)$	0.8	0.5	0.3	0.23	0.13	0.07	0.05	0.035	0.025	0.015	0.009	0
$\frac{d^2y}{dk\,d\Omega}(\Theta=12°)$ $\left[\frac{\text{photons}}{\text{ster Mev electr.}}\right]$	0.4	0.25	0.13	0.09	0.05	0.035	0.025	0.018	0.012	0.008	0.0045	0

1st line: photon energies

2nd-3rd lines: linear absorption coefficients for lead, copper and iron (Ref./29/)

4th-5th lines: transmission for the inside and outside channels (+3 cm Pb) in Fig.16

6th-7th lines: photon yield for 10 MeV electrons on thick W target /23/

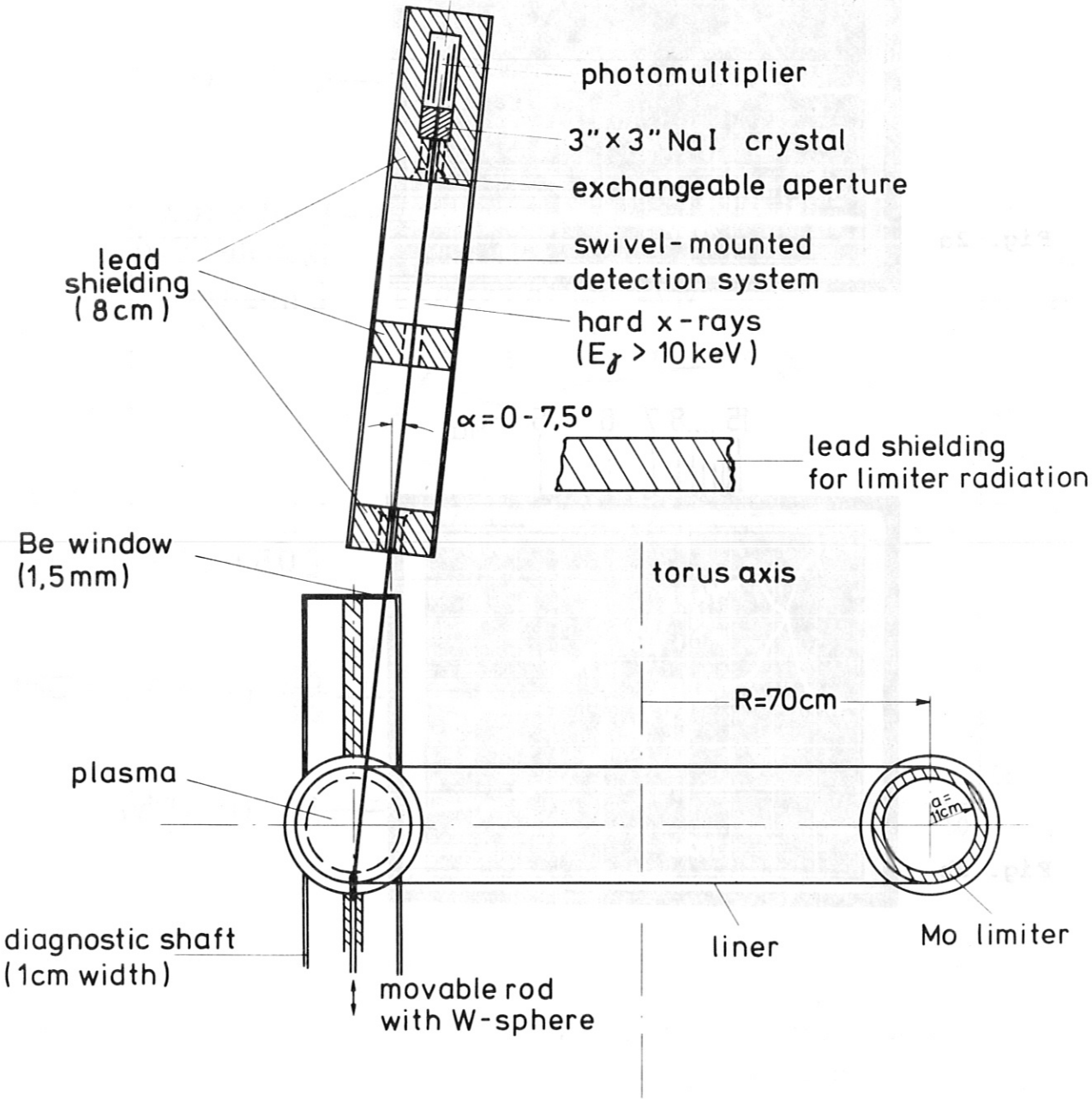

Fig.1: The hard X-ray diagnostic systems for the investigation of plasma bremsstrahlung.

Fig. 2a

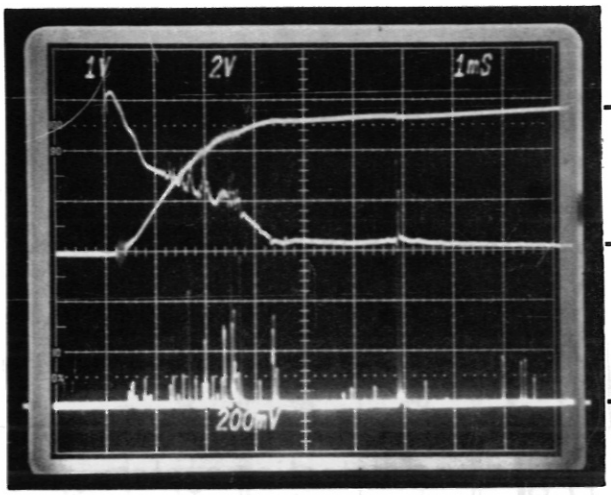

I_p (15.8 KA/Div)

U_L (20 V/Div)

Hard x-Rays
(230 KeV/Div)
[1ms/Div]

Fig. 2b

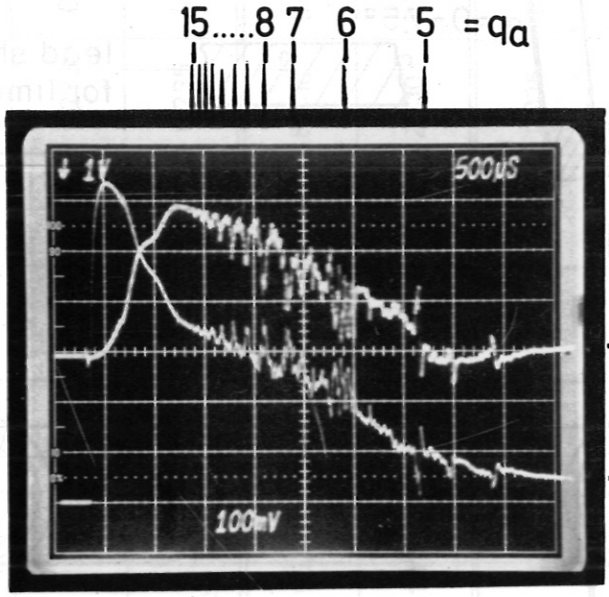

[0.5 ms/Div]

$\frac{dI_p}{dt}$ (7.9 KA/ms/Div)

U_L (10V/Div)

Fig.2: The initial phase of the discharge.

a) Plasma current, loop voltage and hard X-ray pulses.

b) Derivative of plasma current and loop voltage with higher time resolution showing spikes at integer values of the safety factor.

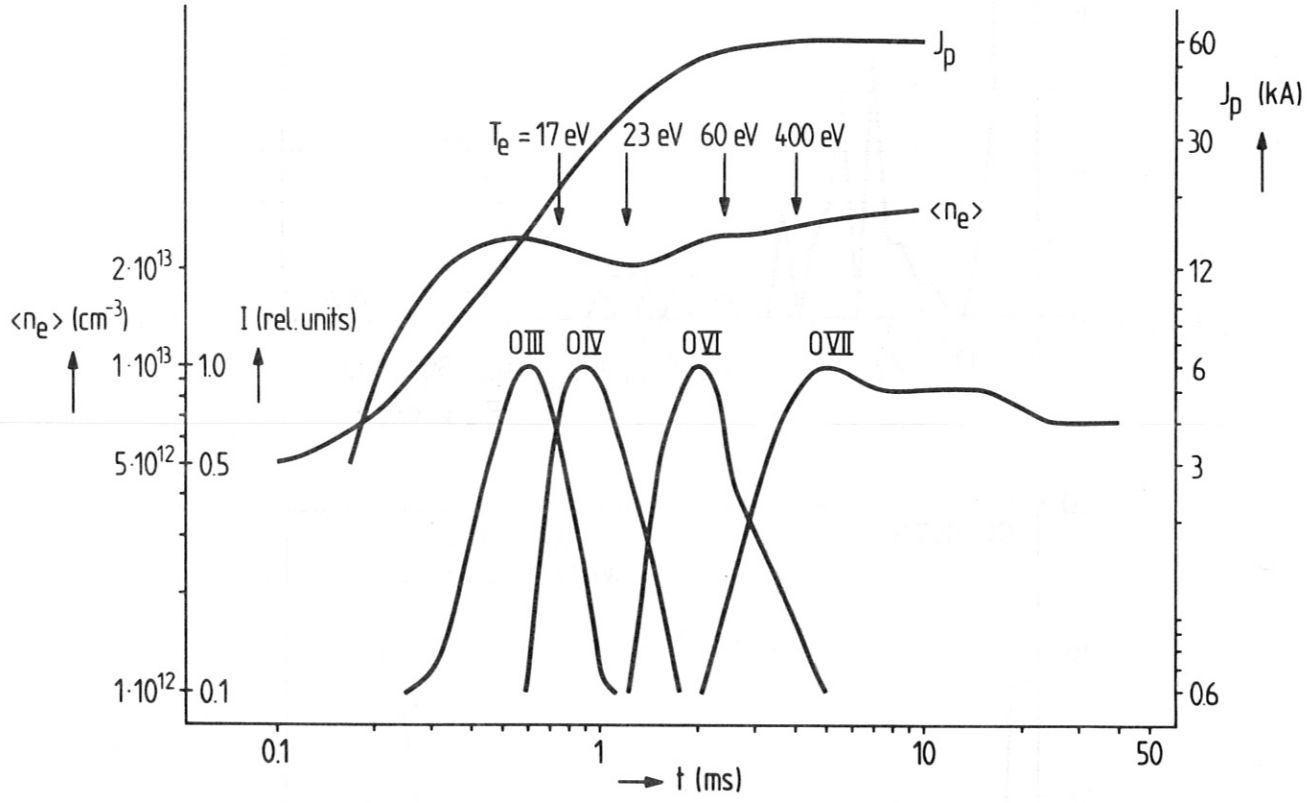

Fig.3: Log-log plot of plasma current, mean electron density, and normalized oxygen intensities from which the first three values of the electron temperature have been estimated /3/. The T_e = 400 eV point has been obtained by laser scattering.

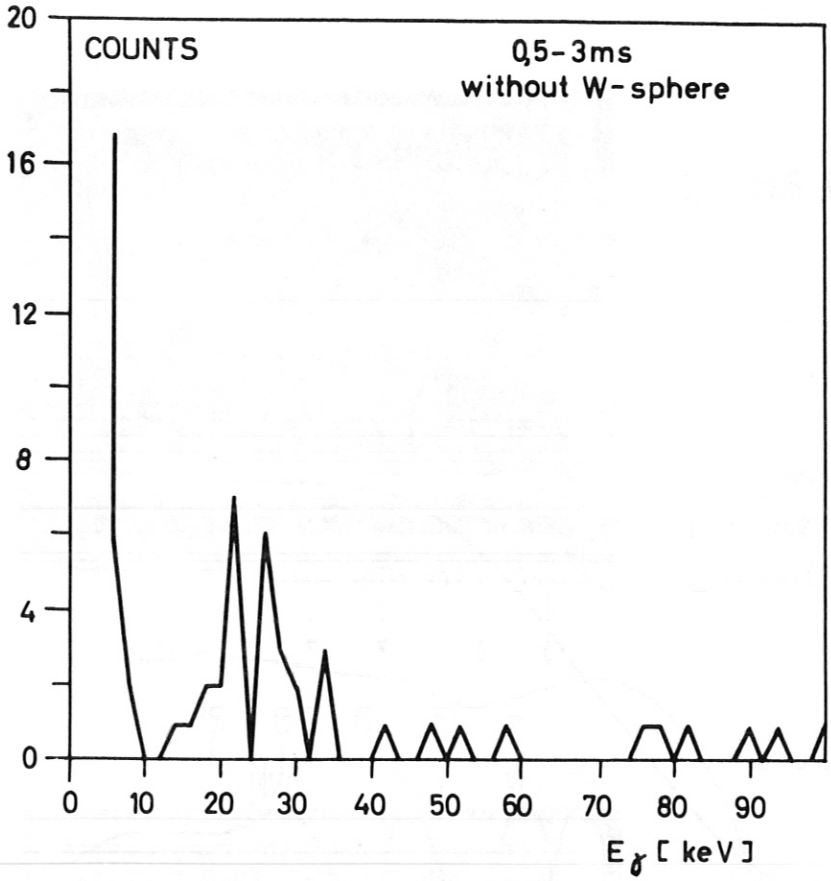

Fig. 4a

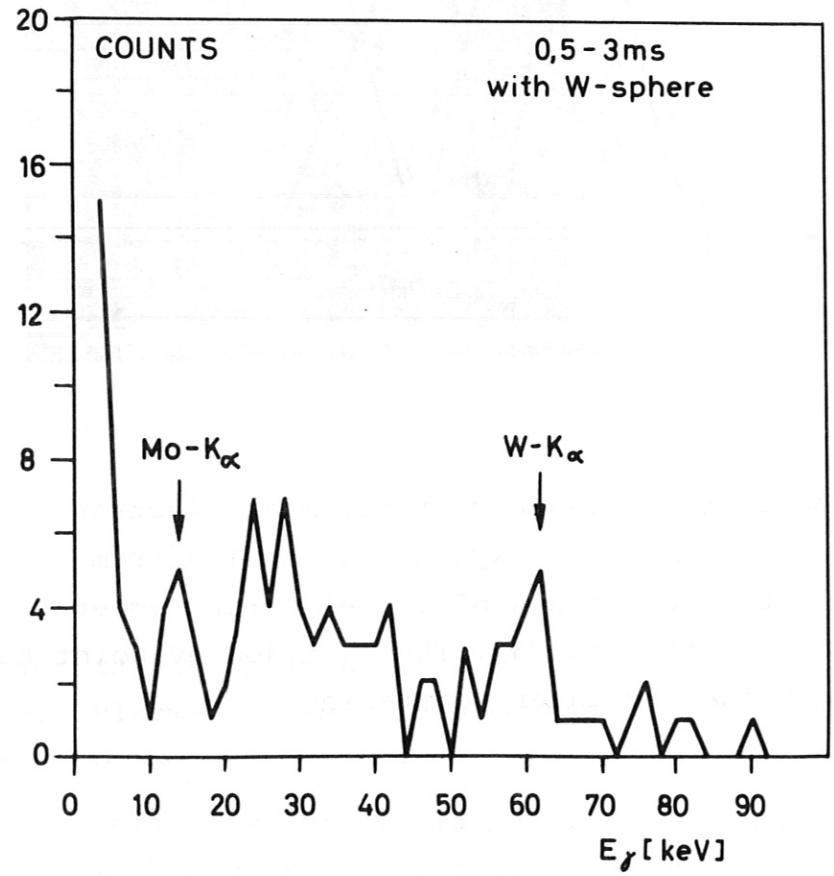

Fig. 4b

Fig.4: Spectra for the time interval 0.5 - 3 ms.

a) without,

b) with tungsten sphere in position. (The peaks around 25 keV could not be identified).

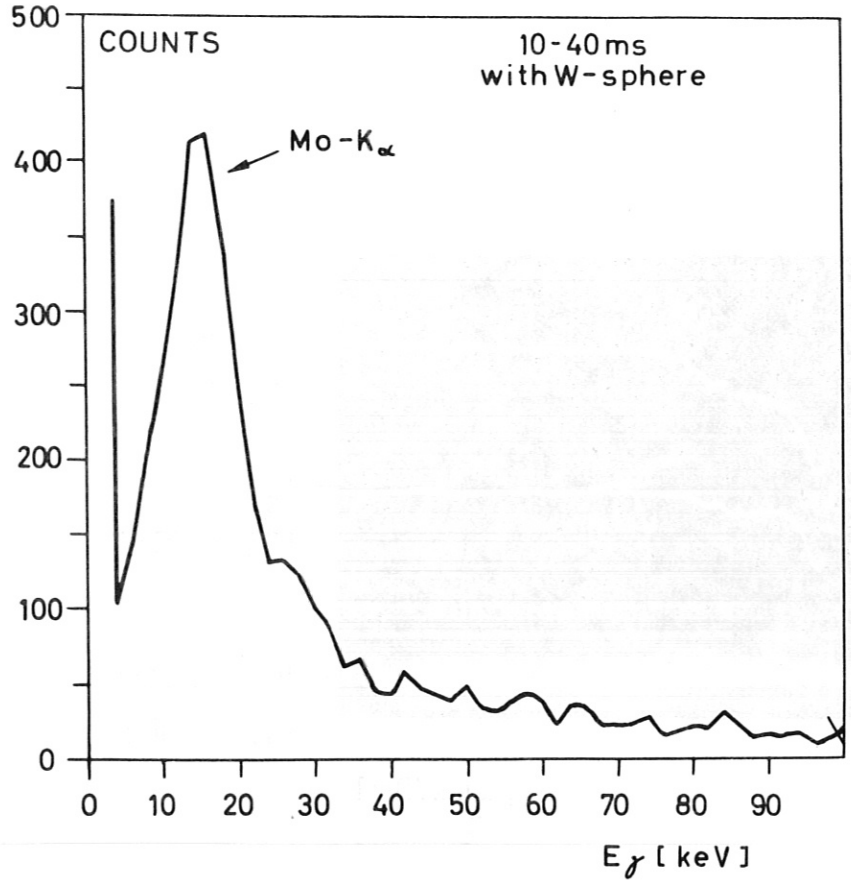

Fig. 5a

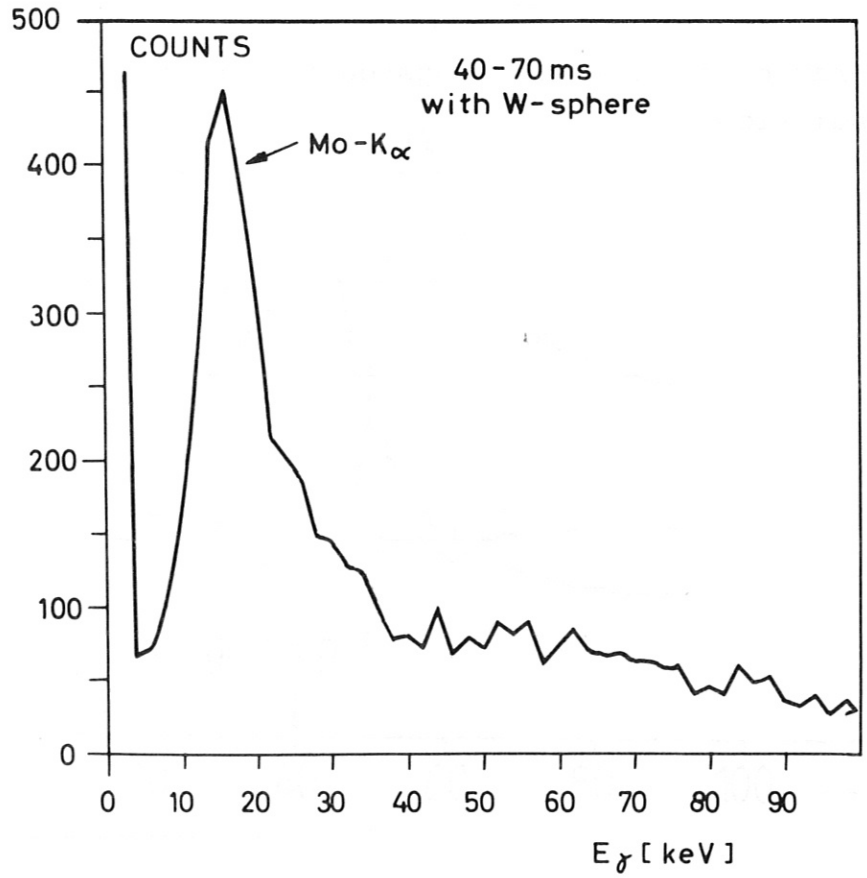

Fig. 5b

Fig.5: Spectra with the tungsten sphere in position.

a) 10 - 40 ms

b) 40 - 70 ms

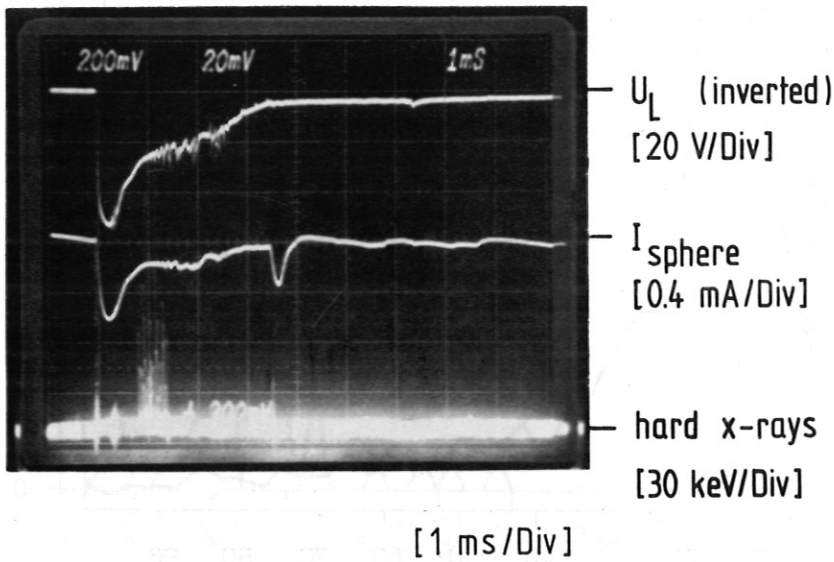

Fig.6: X-ray burst from the tungsten sphere showing W-K_α-radiation.

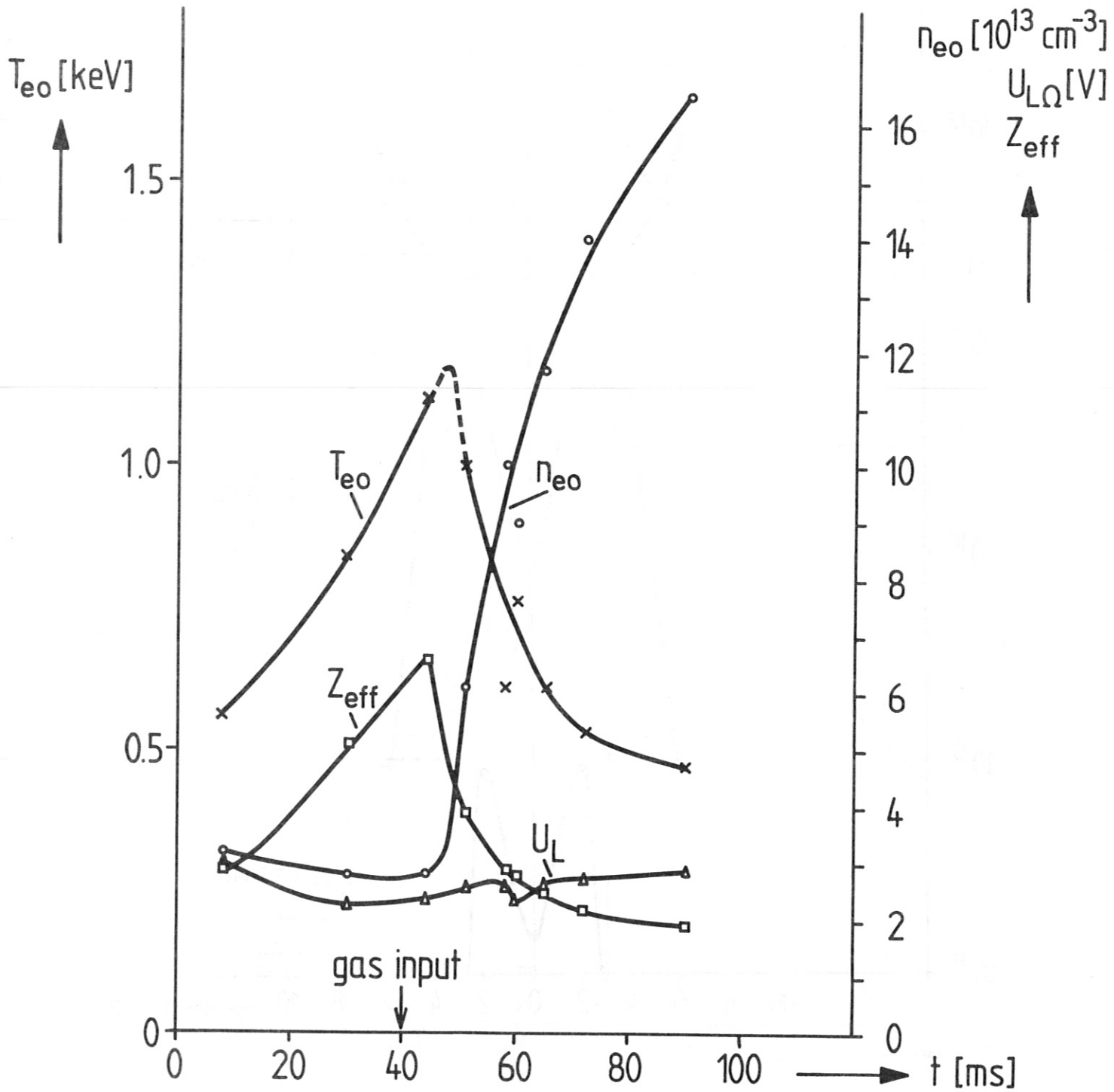

Fig.7: The four parameters defining the runaway production as a function of time.

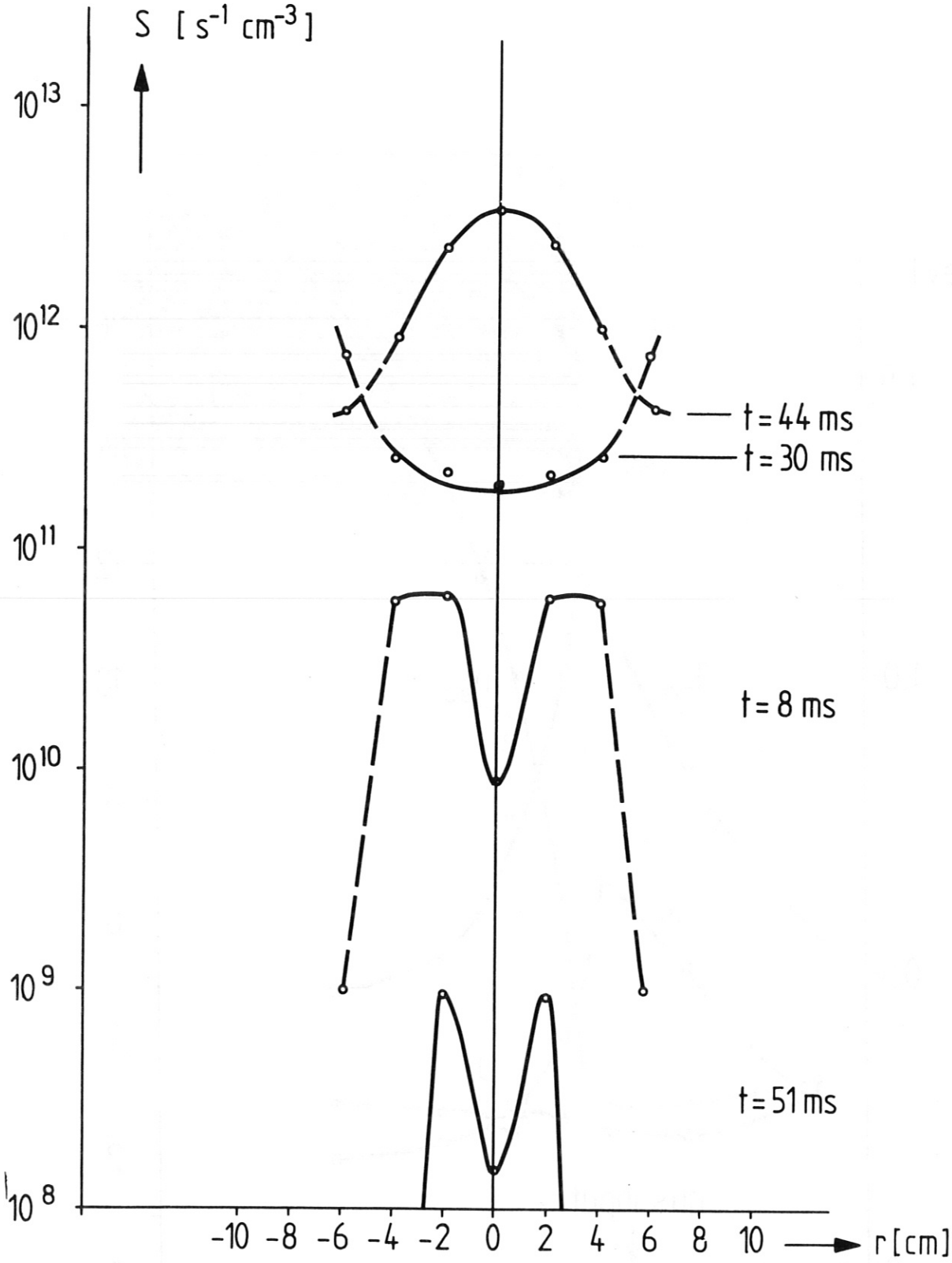

Fig.8: Profiles of the runaway production rate calculated from Thomson scattering data.

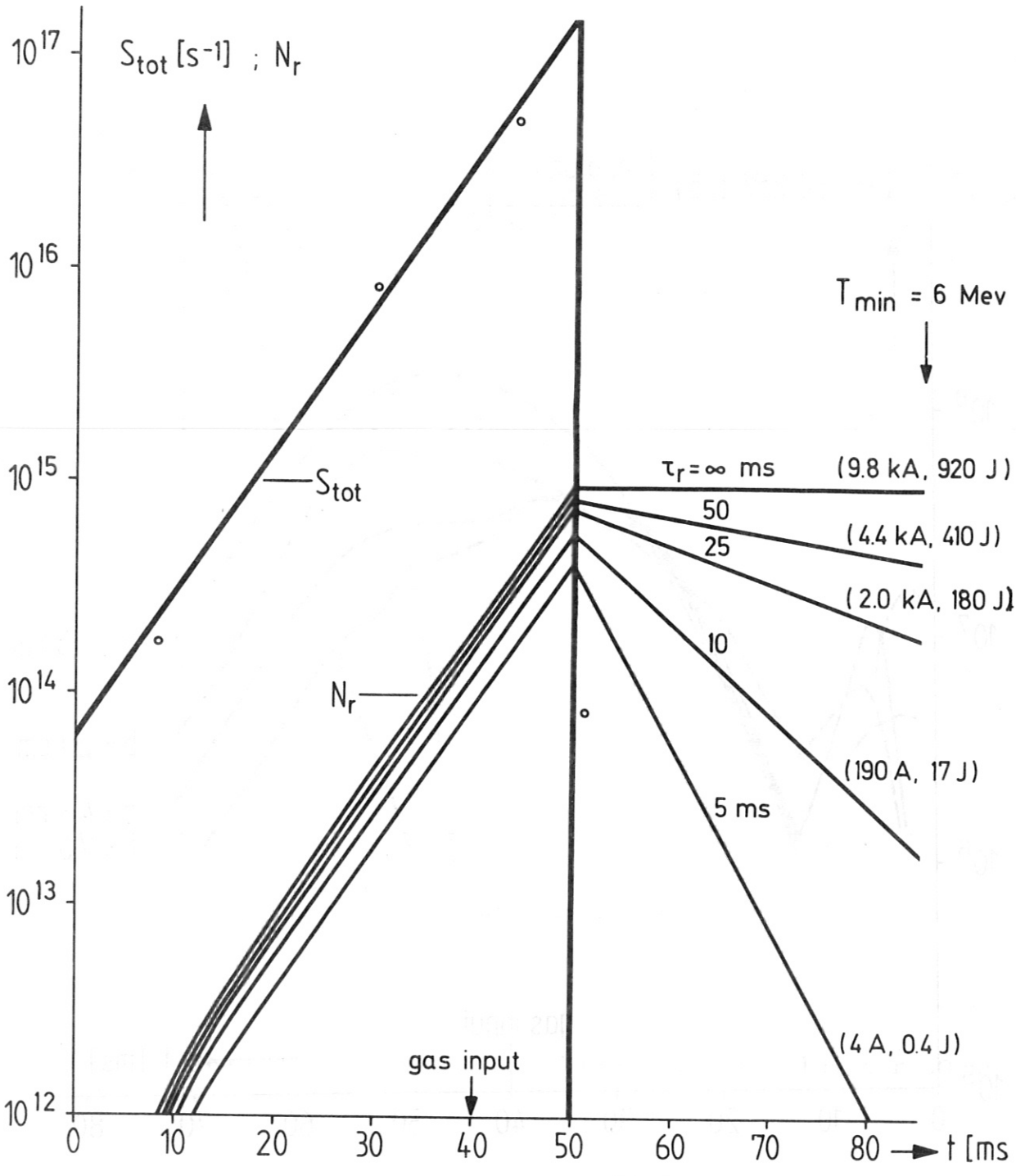

Fig.9: Total runaway production rate and the total number of runaways versus time with the runaway confinement time as a parameter. Also given: the minimum kinetic energy, the runaway current and energy contents at 85 ms.

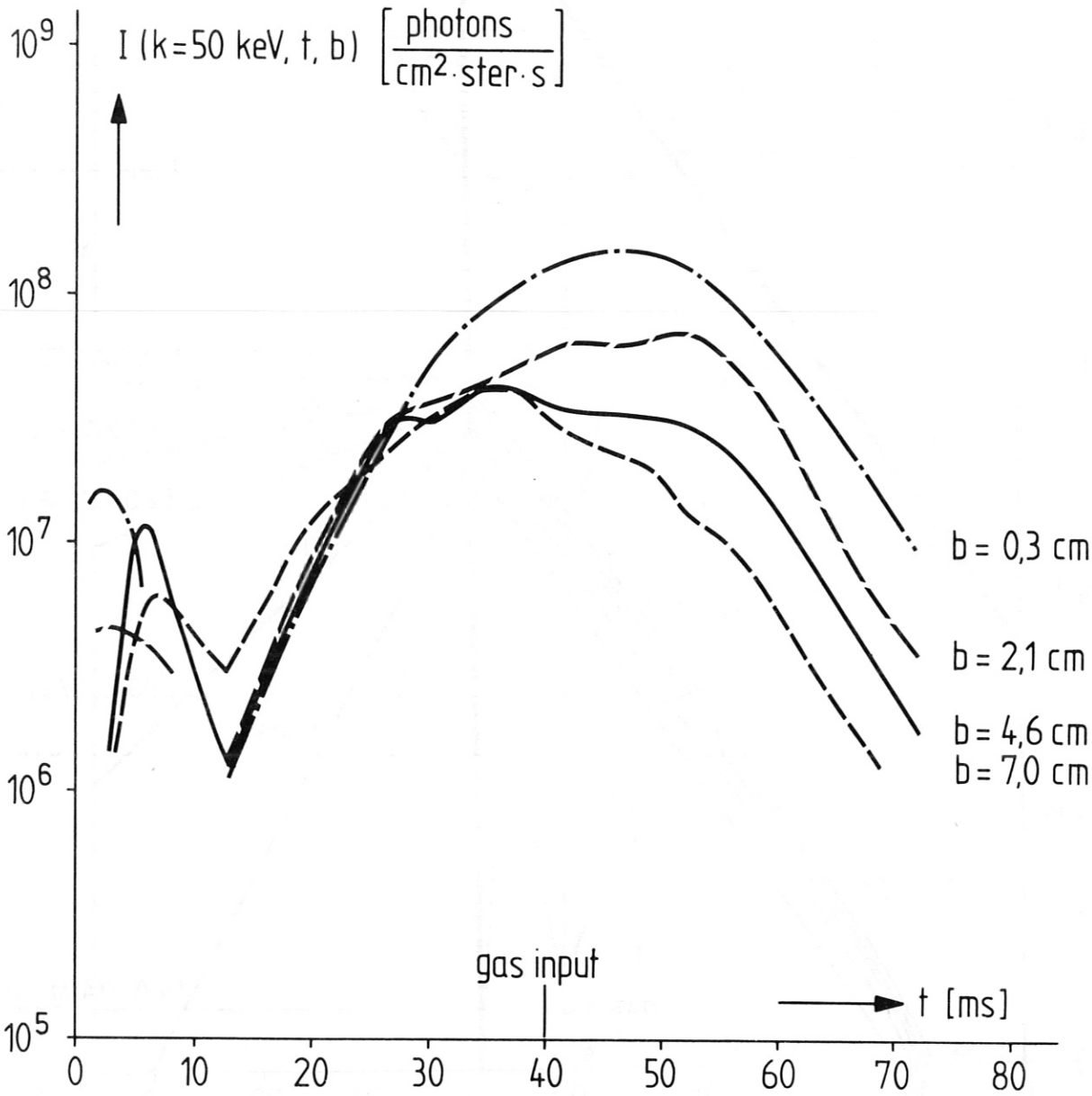

Fig.10: X-ray intensities for 50 keV photons versus time with the chord distance as a parameter.

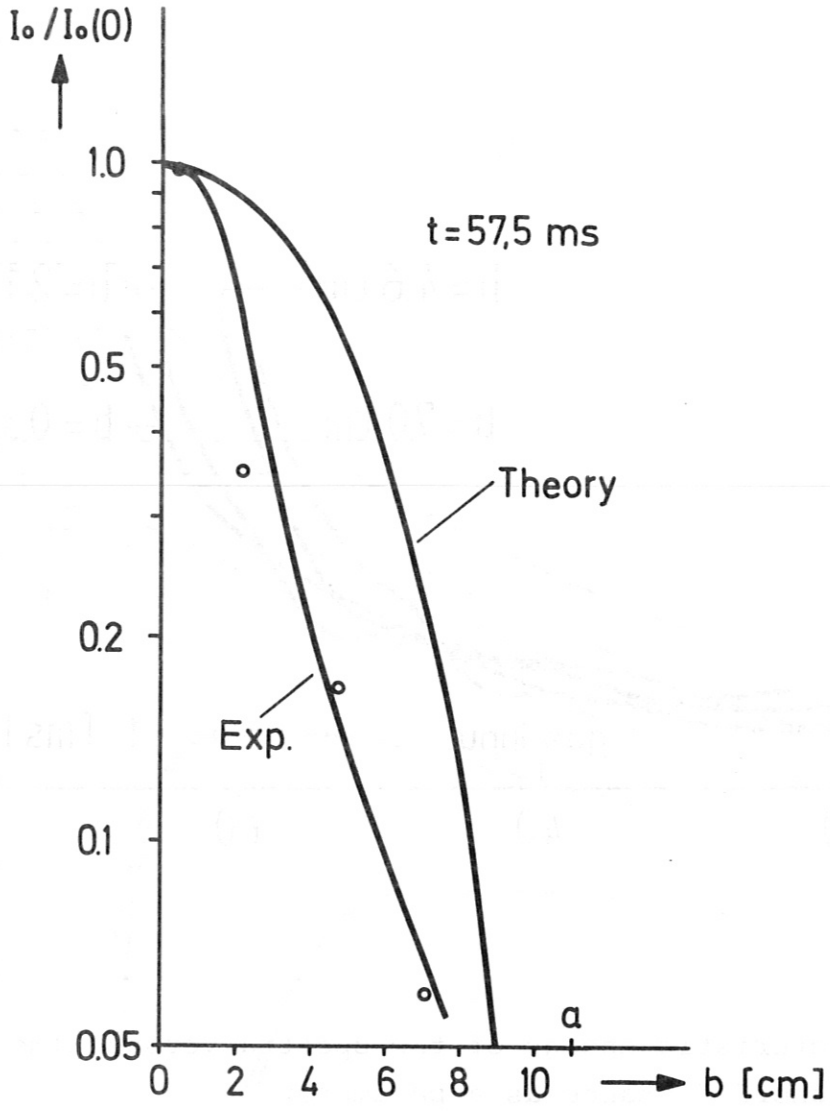

Fig.11: Measured and theoretical intensity profiles for 50 keV photons.

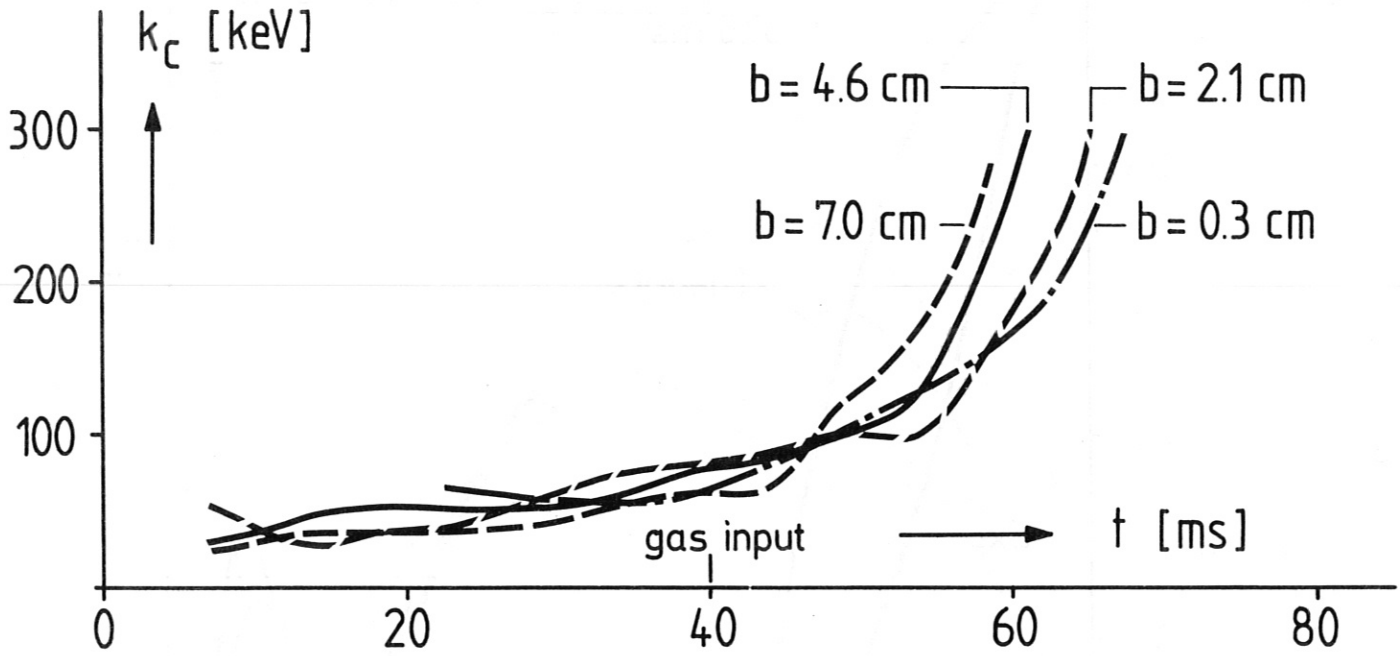

Fig.12: The characteristic energy of the spectra versus time with the chord distance as a parameter.

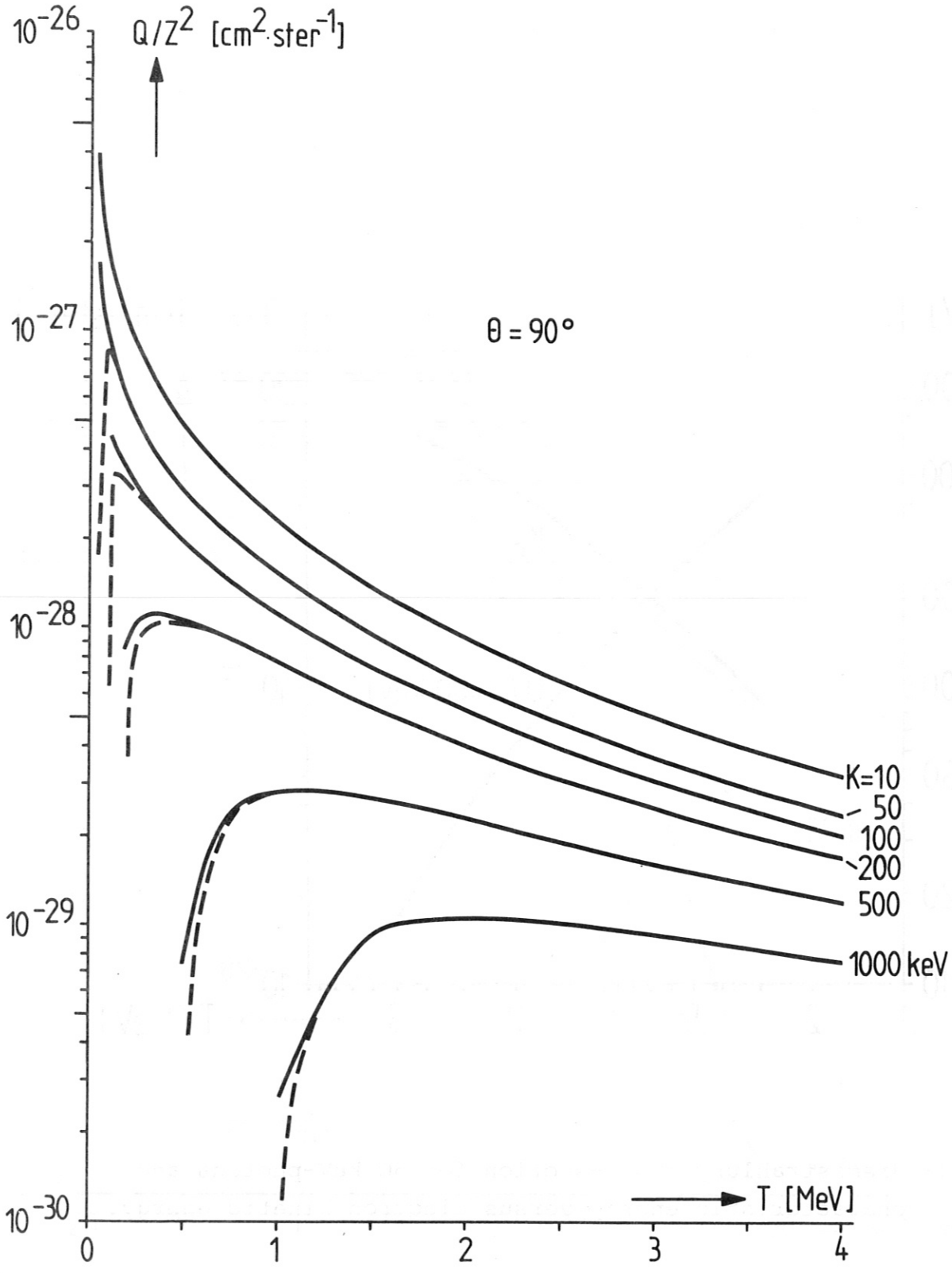

Fig.13: The bremsstrahlung cross-section for $\theta = 90^{\circ}$ as a function of kinetic energy with the photon energy as a parameter (solid lines with, dashed lines without Elwert correction).

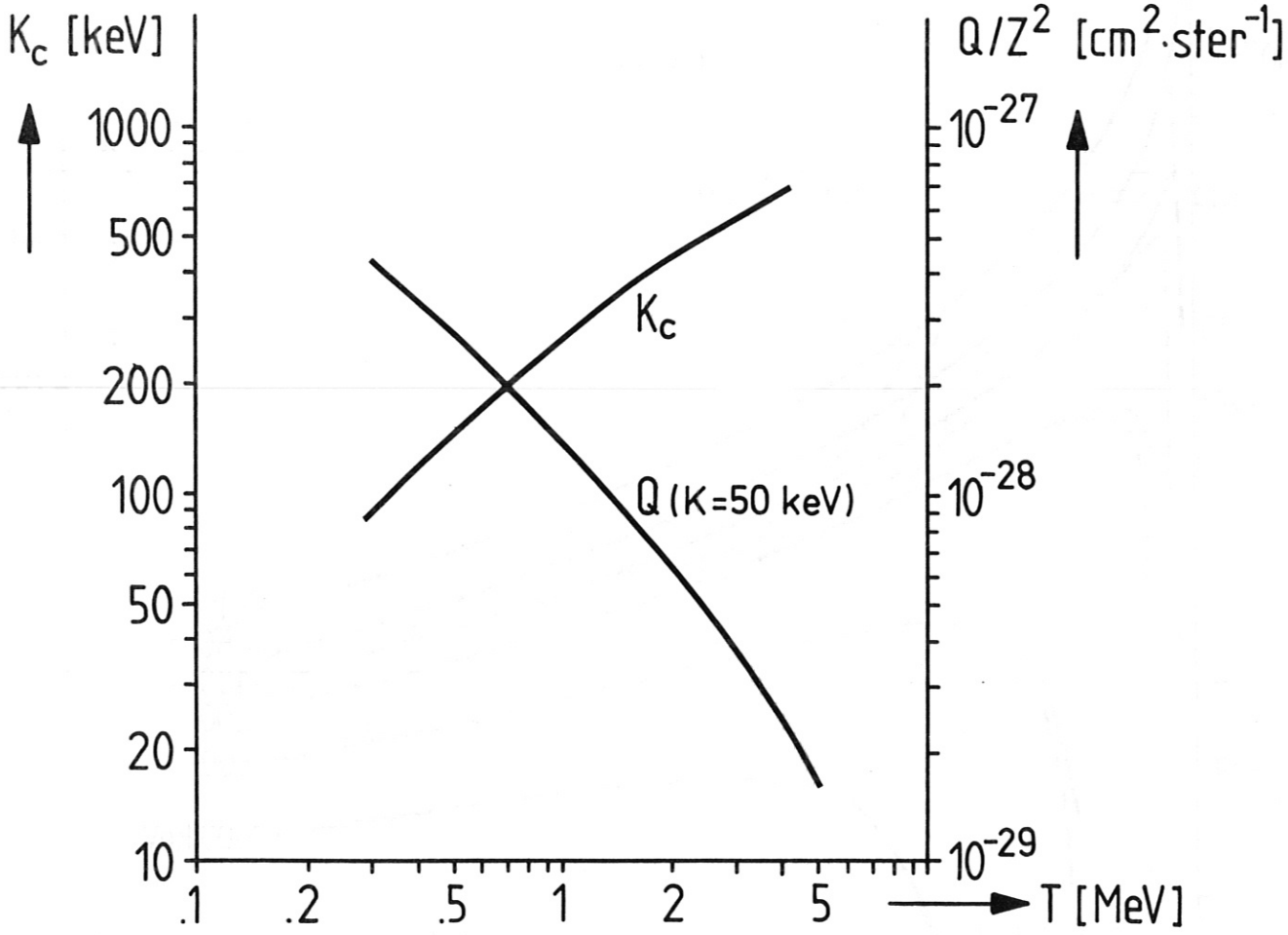

Fig.14: Bremsstrahlung cross-section for 50 keV-photons and characteristic energy versus electron kinetic energy.

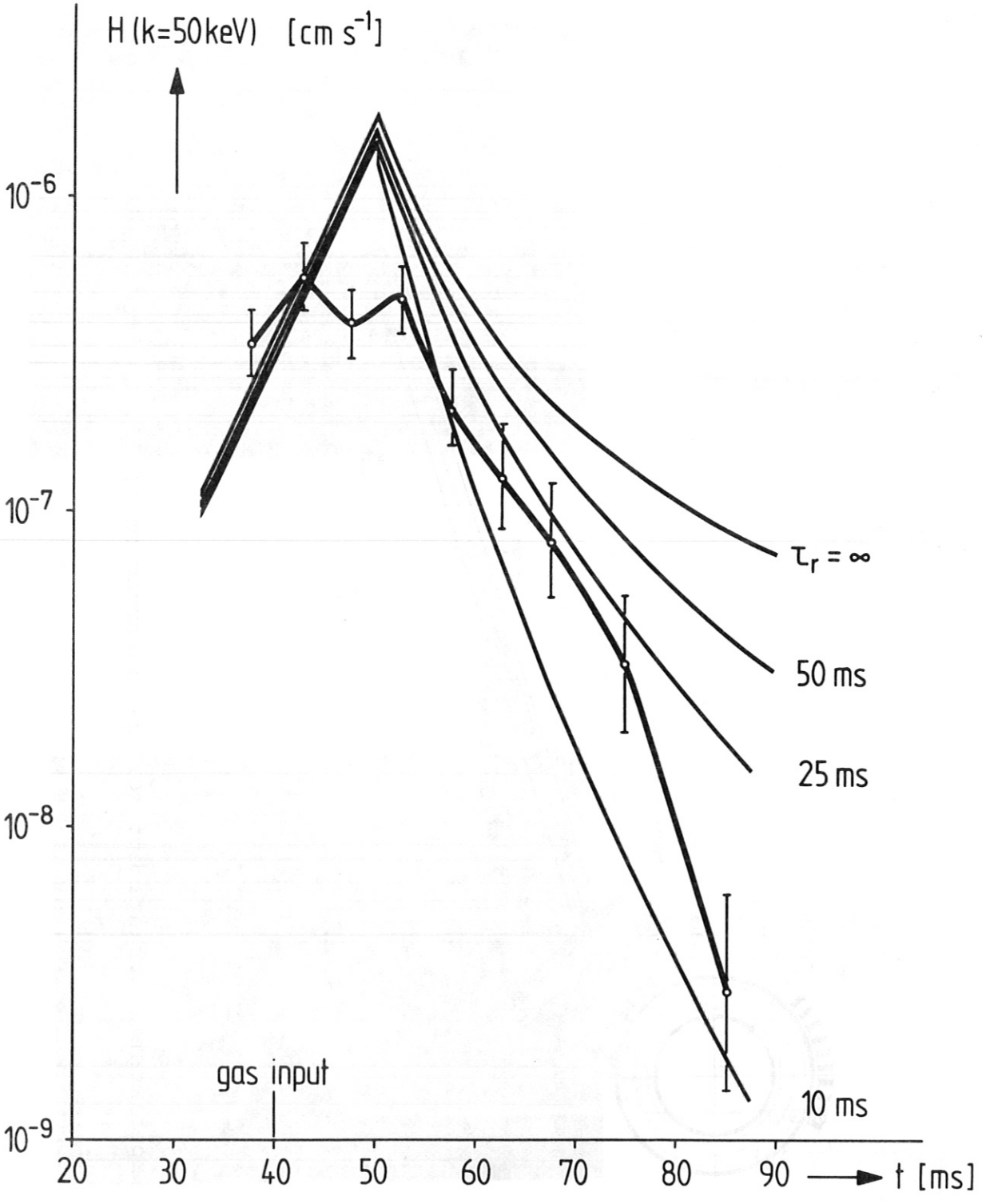

Fig.15: The normalized intensity for 50 keV photons in comparison with theoretical results for various values of the run-away confinement time.

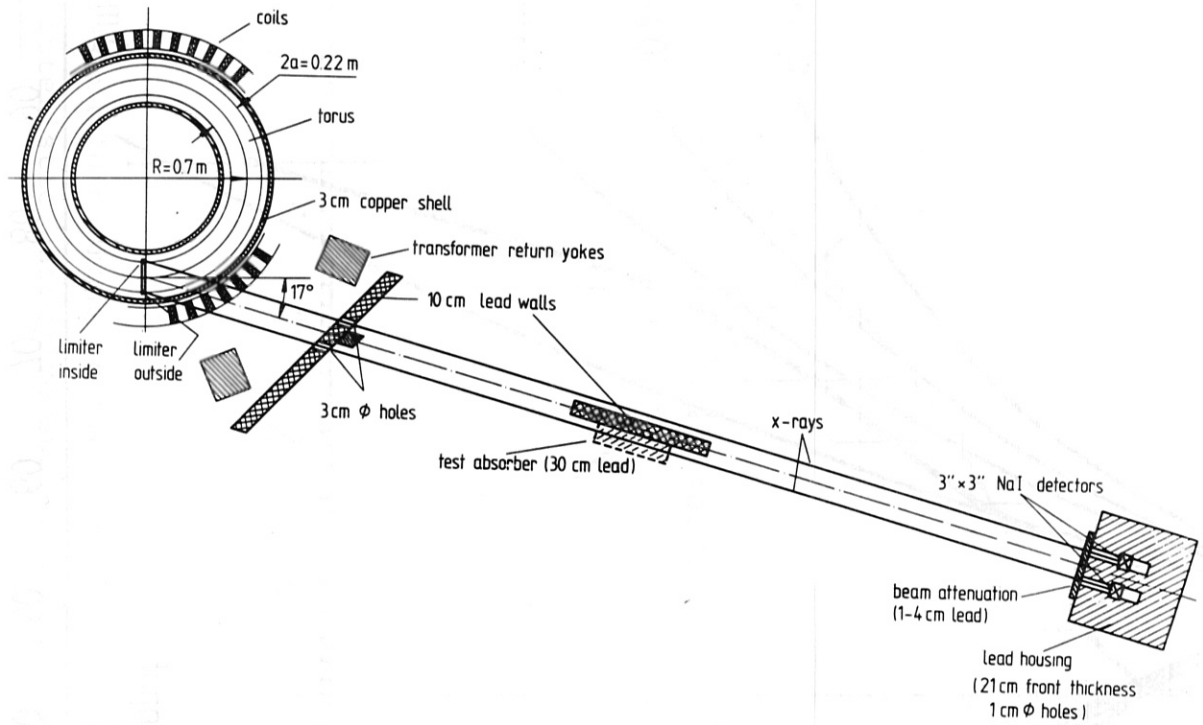

Fig.16: Experimental arrangement for the observation of limiter radiation.

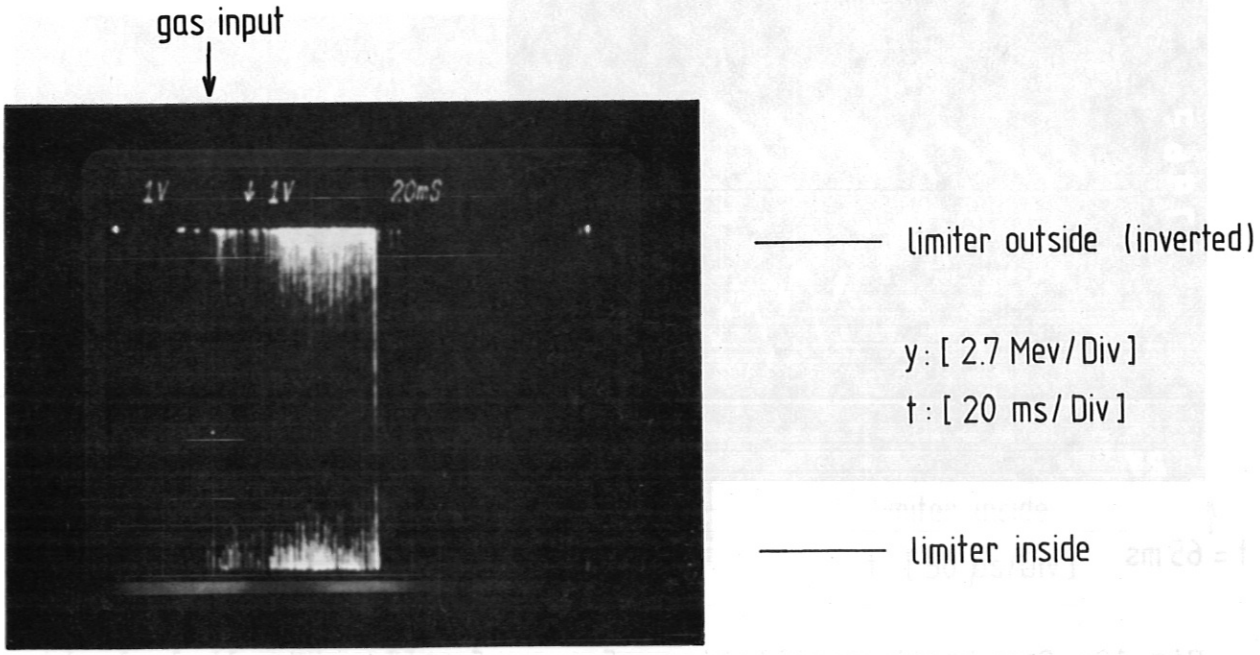

Fig.17: X-ray pulses as a function of time obtained with set-up shown in Fig.16.

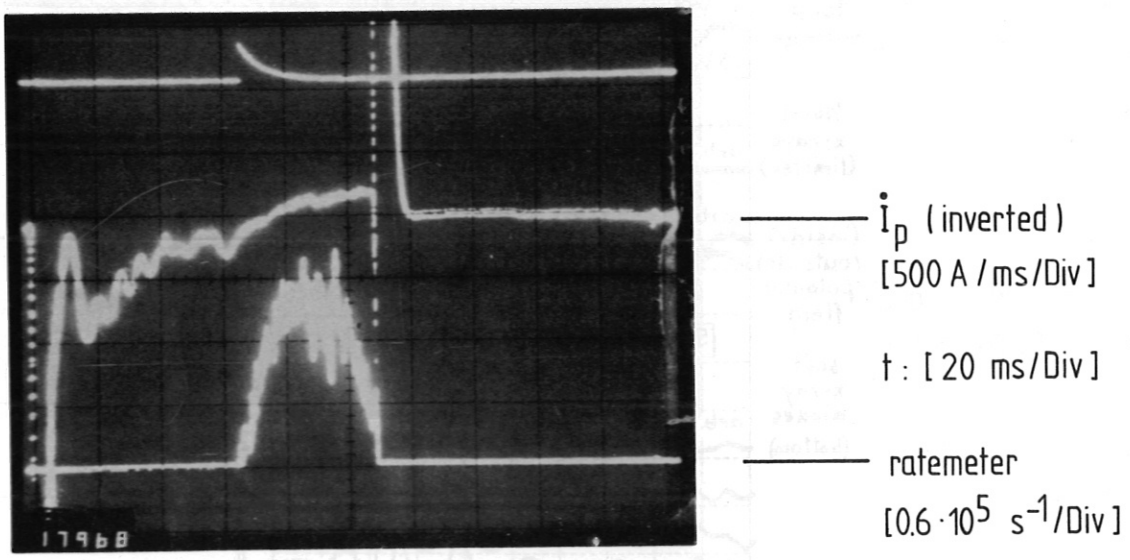

Fig.18: Hard X-ray intensity ($k \gtrsim 500$ keV) and derivative of plasma current as a function of time.

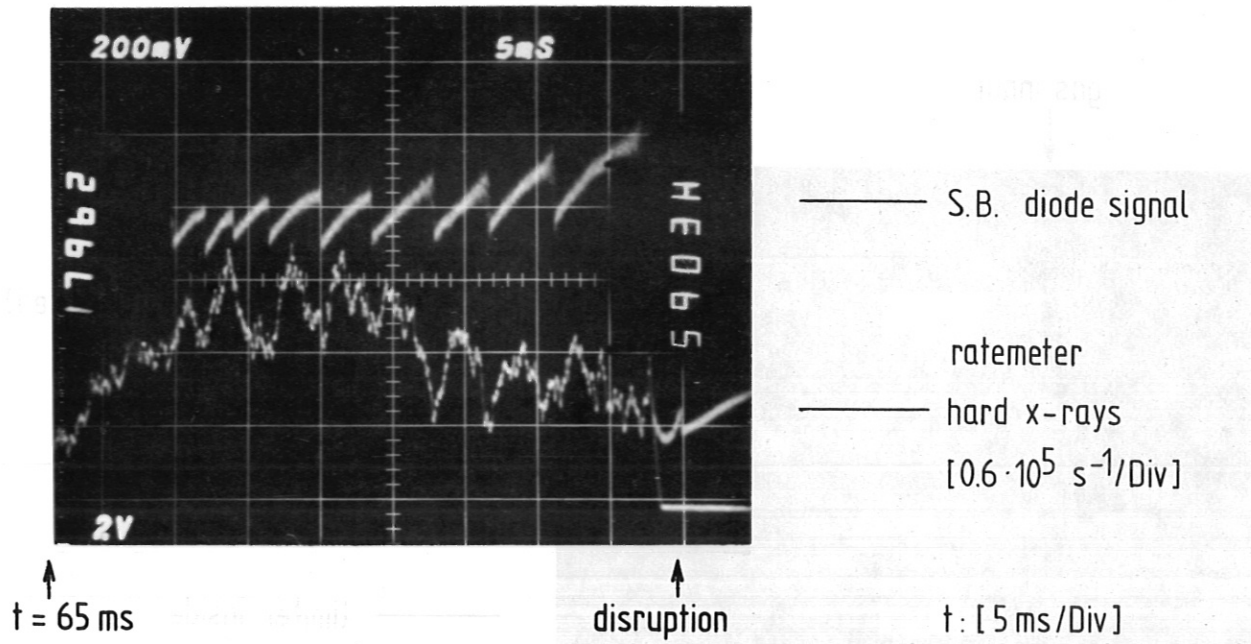

Fig.19: Saw tooth oscillation of a surface barrier diode looking to the plasma center and hard intensity ($k \gtrsim 1$ MeV) of limiter radiation showing inverse saw tooth (1 ms integration time)

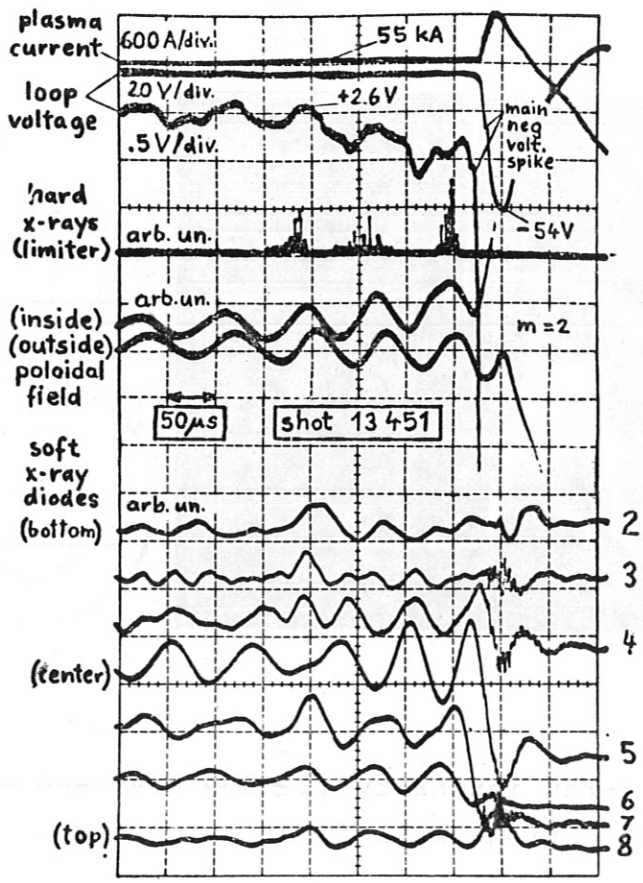

Fig.20: A time interval of 500 μs at the disruption.

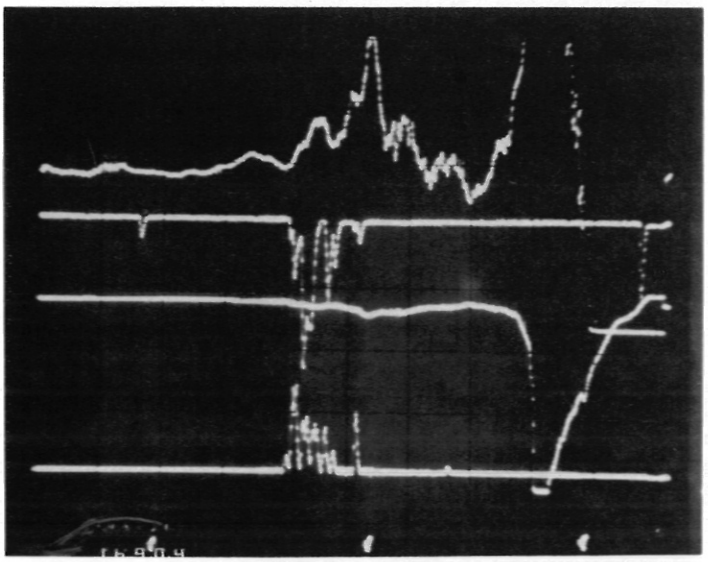

—— $\dot{I}_p$ [$3.2 \cdot 10^6$ As^{-1}/Div]

—— x-rays [5.4 Mev/Div]
limiter outside

—— U_{Loop} [20 V/Div]

—— x-rays [5.4 Mev/Div]
limiter inside

t : [50 µs/Div]

Fig. 21a

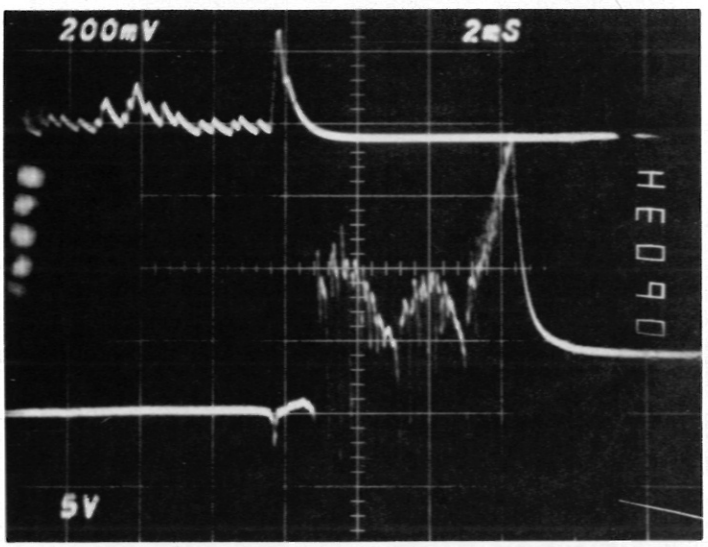

—— pulse-rate [$1.5 \cdot 10^4$ s^{-1}/Div]
limiter outside

—— U_{Loop} [10 V/Div]

t : [2 ms/Div]

Fig. 21b

Fig.21: The disruption seen in high (a) and low (b) time resolution.